Neutrino – nucleon reaction rates in the supernova core in the relativistic random phase approximation

Shoichi Yamada
Department of Physics, Graduate School of Science, University of Tokyo, 7-3-1, Hongo, Bunkyo-ku, Tokyo 113-0033

Hiroshi Toki
Research Center for Nuclear Physics (RCNP), Osaka University, Ibaraki, Osaka 567-0047, Japan

(February 1, 2008)

arXiv:astro-ph/9907044v1 5 Jul 1999

In view of the application to supernova simulations, we calculate neutrino reaction rates with nucleons via the neutral and charged currents in the supernova core in the relativistic random phase approximation (RPA) and study their effects on the opacity of the supernova core. The formulation is based on the Lagrangian employed in the calculation of nuclear equation of state (EOS) in the relativistic mean field theory (RMF). The nonlinear meson terms are treated appropriately so that the consistency of the density correlation derived in RPA with the thermodynamic derivative obtained from EOS by RMF is satisfied in the static and long wave length limit. We employ pion and rho meson exchange interactions together with the phenomenological Landau – Migdal parameters for the isospin-dependent nuclear interactions. We find that both the charged and neutral current reaction rates are suppressed from the standard Bruenn's approximate formula considerably in the high density regime ($\rho_b \gtrsim 10^{14}$g/cm^3 with ρ_b the baryonic density). In the low density regime ($\rho_b \lesssim 10^{14}$g/cm^3), on the other hand, the vector current contribution to the neutrino – nucleon scattering rate is enhanced in the vicinity of the boundary of the liquid – gas phase transition, while the other contributions are moderately suppressed there also. In the high temperature regime ($T \gtrsim 40$MeV with T the temperature) or in the regime where electrons have a large chemical potential, the latter of which is important only for the electron capture process and its inverse process, the recoil of nucleons cannot be neglected and further reduces the reaction rates with respect to the standard approximate formula which discards any energy transfer in the processes. These issues could have a great impact on the neutrino heating mechanism of collapse-driven supernovae.

I. INTRODUCTION

Calculations of neutrino – nucleon reaction rates in a hot ($T \lesssim 50$MeV) and dense (10^{13}g/cm$^3 \lesssim \rho_b \lesssim 10^{15}$g/cm^3) core of a collapse-driven supernova are complicated problems (see, e.g., [1–3] for the standard rates). When the density reaches $\rho_b \sim 10^{13}$g/cm^3, the average separation of nucleons $d \sim 6\times10^{-13}$cm $(\rho_b\,/\,10^{13}\text{g/cm}^3)^{-1/3}$ becomes of the same order as the typical neutrino compton wave length $\lambda_\nu \sim 6\times10^{-13}$cm $(E_\nu\,/\,30\text{MeV})^{-1}$. This means that neutrinos are interacting simultaneously with multiple nucleons for this density or higher. If nucleons are distributed uniformly in space and time, which is unlikely, the outgoing waves from multiple targets interfere with one another and the cross sections remain the product of the number of targets and the cross section of a single scattering. However, in reality, the distributions of nucleons are fluctuating due to mutual interactions and the reaction rates will be modified from those obtained with this simple formula. Furthermore, the typical energy $E_\nu \sim 30$MeV $(T/10\text{MeV})$ of a neutrino, which is approximately an inverse of the duration time of interaction between a neutrino and a nucleon, is of the same order as the nucleon – nucleon scattering rate $\Gamma \sim \langle\sigma v\rangle n_b \sim 30$MeV for the density $\rho_b \sim 3\times10^{13}$g/cm^3 and temperature $T \sim 10$MeV, where σ, v and n_b are the scattering cross section, the nucleon velocity and the nucleon number density. This implies that while a neutrino is interacting with a nucleon, the target nucleon is scattered off by another nucleon. Hence both the spatial and temporal correlations of nucleons are important.

It is, however, very difficult to calculate these correlations of nucleons accurately, since they are induced by the strong nuclear interactions and cannot be treated with a simple perturbation. This issue was studied by several authors from early on. Sawyer [4], for example, calculated the density and spin-density fluctuations of nuclear matter in the static and long wave length limit from an equation of state, while Iwamoto & Pethick [5] investigated them from the Fermi liquid theory. These results have not been incorporated extensively in simulations of supernovae or proto neutron stars (see, however, [6]) and the simpler formula mentioned above of the reaction rates has been used even in the most sophisticated computations. [7–10]

With increasing recognition that the neutrino transport is one of the key factors for a successful supernova explosion [11,12], this issue has recently attracted attentions of supernova researchers. In the neutrino heating scenario of

supernova explosion [13,14], which is supposed to be the most promising at present, the shock wave stagnated in the iron core after the core bounce is expected to be revigorized by neutrinos diffusing out of the proto neutron star. It has been shown that it is important in this mechanism to increase the neutrino heating rate via the dominant processes of electron neutrino absorption on neutrons and electron antineutrino absorption on protons behind the shock wave. This heating rate is approximately given by:

$$Q_\nu \approx 110 \cdot \frac{L_{\nu,52}\langle E^2_{\nu,15}\rangle}{r_7^2\langle\mu\rangle} \cdot \left\{ \begin{array}{c} Y_n \\ Y_p \end{array} \right\} \quad \left[\frac{\mathrm{MeV}}{\mathrm{sec}\cdot N_b}\right] \quad . \tag{1.1}$$

Here $Y_n = n_n/n_b$ and $Y_p = n_p/n_b$ are the number fractions of free neutrons and protons, respectively; the normalization with the baryonic number density n_b indicates that the rate per baryon is calculated in Eq. (1.1); $L_{\nu,52}$ denotes the neutrino luminosity in units of 10^{52}erg/s, $E_{\nu,15}$ the neutrino energy normalized by 15MeV, r_7 the radius in 10^7cm; $\langle\mu\rangle$ is the mean value of the cosine of the angle of neutrino propagation relative to the radial direction. It is clear from this equation that the higher neutrino energy and/or the greater neutrino luminosity increase the neutrino heating rate. One obvious way to achieve that is to decrease the neutrino opacities in the supernova core. Since the dominant source of opacity for neutrinos is the neutrino – nucleon reactions, the modifications of their rates could have a great impact on the supernova mechanism [15–20].

As stated above, the neutrino – nucleon reaction rates used in the supernova simulations thus far were mostly evaluated by multiplying the rate for a single target nucleon with the nucleon number density (see, e.g., [2,21] and references therein), thus ignoring the correlations due to ambient nucleons. Recently, however, some authors [18–20,22,23] calculated the density as well as the spin-density correlations of nucleons due to nuclear forces based on RPA. As shown later, this method evaluates the nonuniform nucleon distributions in space and time using the mean field approximation. On the other hand, Raffelt and his company [15,16,24–26] insisted that the effect from collisions of two nucleons on the nucleon spin-density fluctuations cannot be neglected, which is not taken into account in RPA (see also [27]).

One of the authors (H. T.) recently published the nuclear EOS based on RMF and the Thomas – Fermi approximation for finite nuclei covering the wide range of density, temperature and electron fraction of relevance to the supernova simulations [28,29]. In this paper, we calculate the nuclear correlations in the relativistic RPA based on the Lagrangian used in the calculation of EOS in RMF [30,31]. It is shown in the next section that this guarantees the thermodynamical consistency of the neutral vector current part of reaction rates with EOS in the static and long wave length limit if the nonlinear meson terms are appropriately treated. The neutral axial vector current and the charged current contributions to reaction rates are calculated on the same basis but with additional introduction of the phenomenological Landau – Migdal parameters for the isovector channel [32,34,35,57], since they do not contribute to RMF and are neglected in the theory. The possible collisional effects which are supposed to be important particularly in the low density regime and might have some roles in forming the neutrino spectra will be discussed elsewhere [36], since we consider the consistency of the reaction rates with EOS which we have currently at hand is more important.

This paper is organized as follows. In the next section we formulate the neutrino reaction rates with nucleons by the so-called dynamical structure functions and show that RPA is consistent with EOS obtained by the mean field theory. Then we represent some modifications of the reaction rates due to the RPA correlations, using the Bruenn's standard aprroximation formula as a reference. We summarize the paper with some discussions of implications for the supernova simulations in the last section.

II. NEUTRINO – NUCLEON REACTION RATES

First we express the reaction rates in a general form. Since we are interested in low energy reactions ($E \ll M_w$, the mass of weak boson), the weak interaction is well approximated by the interaction Lagrangian density:

$$\mathcal{L}_I(x) = \frac{G_F}{\sqrt{2}}\, l_\mu(x)\; J^\mu_N(x) \quad , \tag{2.1}$$

where G_F is the Fermi coupling constant, $l_\mu(x)$ is the lepton weak current given by

$$l_\mu(x) = \overline{\psi}_l(x)\; \gamma^\mu(1-\gamma_5)\; \psi_l(x) \quad , \tag{2.2}$$

and $J^\mu_N(x)$ is the nucleon counter part,

$$J^\mu_N(x) = \overline{\psi}_N(x)\; \gamma^\mu(h_V - h_A\gamma_5)\; \psi_N(x) \quad . \tag{2.3}$$

h_V and h_A are the vector and axial vector coupling constants, respectively, and are taken for the charged current as $h_V = g_V = 1$ and $h_A = g_A = 1.23$. For the neutral current they are $h_V^n = -1/2$, $h_A^n = -1/2\, g_A$ and $h_V^p = 1/2 - 2\sin^2\theta_W$, $h_A^p = 1/2\, g_A$ for neutron and proton, respectively. θ_W is the Weinberg angle.

Following the standard procedure (see, e.g., [37]), the reaction rates are obtained by making a square of each matrix element evaluated up to the lowest order of the Fermi coupling constant, taking the thermal ensemble average for the initial state and summing over the final states:

$$R\,(q^{in},\, q^{out}) \;=\; \frac{G_F^2}{2}\; K_{\alpha\beta}\,(q^{in},\, q^{out})\; S_N^{\alpha\beta}(k) \quad . \tag{2.4}$$

q^{in} and q^{out} are the four momenta of the incident and outgoing leptons, respectively. $k = q^{in} - q^{out}$ is the four momentum transferred from lepton to nucleon. In the above equation, the tensor $K_{\alpha\beta}$ comes from the kinematics of leptons and given by

$$K_{\alpha\beta}\,(q^{in},\, q^{out}) \;=\; 8\,(q_\alpha^{out} q_\beta^{in} \;+\; q_\beta^{out} q_\alpha^{in} \;-\; q^{out}\cdot q^{in}\, g_{\alpha\beta} \;+\; i\,\varepsilon_{\alpha\beta}{}^{\delta\gamma}\, q_\delta^{out} q_\gamma^{in}) \quad . \tag{2.5}$$

Here $g_{\alpha\beta}$ is the metric tensor with the signature of $[+---]$, and $\varepsilon^{\alpha\beta\delta\gamma}$ is the antisymmetric tensor with $\varepsilon^{0123} = 1$. All information of nucleons is contained in the so called dynamical structure function $S_N^{\alpha\beta}$ defined as:

$$S_N^{\alpha\beta}(k) \;=\; \int d^4x\; e^{ikx}\; \langle\, J_N^\alpha(x)\, J_N^\beta(0)\,\rangle \quad , \tag{2.6}$$

where $\langle\cdots\rangle$ stands for the thermal ensemble average of the argument.

The structure function can be generally decomposed as follows due to the isotropy of the system:

$$\begin{aligned} S_N^{\alpha\beta}(k) \;=\; & R_1(k)\, u^\alpha u^\beta \;+\; R_2(k)\,(u^\alpha u^\beta - g^{\alpha\beta}) \;+\; R_3(k)\, k^\alpha k^\beta \\ & +\; R_4(k)\,(k^\alpha u^\beta + u^\alpha k^\beta) \;+\; i\, R_5(k)\,\varepsilon^{\alpha\beta\delta\gamma}\, u_\delta u_\gamma\,, \end{aligned} \tag{2.7}$$

where u^α is a four velocity of the system. Putting Eqs. (2.5) and (2.7) into Eq. (2.4), we get

$$\begin{aligned} R\,(E^{in},\, E^{out},\, \cos\theta) \;=\; & 4\, G_F^2\, E^{in} E^{out}\; [R_1(k)\,(1+\cos\theta) \;+\; R_2(k)\,(3-\cos\theta) \\ & -\; 2\,(E^{in} + E^{out})\, R_5(k)\,(1-\cos\theta)] \quad , \end{aligned} \tag{2.8}$$

where E^{in} and E^{out} are the energies of the incident and outgoing leptons, and θ is the angle between the incident and outgoing three momenta. There are three terms with different angular dependences. In general the third contribution is much smaller than the other two terms and ignored in the following discussions. The meanings of them become clearer if we take the non-relativistic limit for the nucleon kinematics. In this limit $R_1(k)$ and $R_2(k)$ are reduced to

$$R_1(k) \approx\; h_V^2 \int d^4x\; e^{ikx}\; \langle\, \rho_N(x)\, \rho_N(0)\,\rangle \quad , \tag{2.9}$$

$$R_2(k) \approx\; \frac{h_A^2}{3} \int d^4x\; e^{ikx}\; \langle\, \boldsymbol{s}_N^i(x)\, \boldsymbol{s}_N^i(0)\,\rangle \quad . \tag{2.10}$$

Thus $R_1(k)$ comes mainly from the vector currrent part of the nucleon weak current and is nothing but a density correlation function of nucleons. $R_2(k)$ originates from the axial vector current of nucleon and represents a spin-density correlation function. $\rho_N(x)$ is the nucleon density and $\boldsymbol{s}_N^i(x)$ is the spin density and the spin components i are summed up.

The calculation of the reaction rates is thus reduced to the evaluation of these correlation functions. It is, however, easier in the field theory to treat the time ordered product instead of the ordinary one since we can apply the perturbation theory more easily for the former (see, e.g., [38]). Hence we define the time ordered product of the weak current $\Pi_N^{\alpha\beta}(k)$ corresponding to the dynamical structure function as:

$$i\,\Pi_N^{\alpha\beta}(k) \;=\; \int d^4x\; e^{ikx}\; \langle\, T\, J_N^\alpha(x)\, J_N^\beta(0)\,\rangle \quad , \tag{2.11}$$

where the symbol T stands for the chronological ordering of operators. It is also convenient to consider the corresponding retarded Green function defined as

$$i\,\Pi_N^{R\alpha\beta}(k) \;=\; \int d^4x\; e^{ikx}\; \Theta(t)\; \langle\, [J_N^\alpha(x),\, J_N^\beta(0)]\,\rangle \quad , \tag{2.12}$$

where $[A, B]$ denotes the commutator of A and B and $\Theta(t)$ is the Heaviside function. In fact, the dynamical structure function is related with the imaginary parts of those Green functions via a simple formula:

$$S_N^{\alpha\beta}(k) \;=\; -\,\frac{2}{1+e^{-\beta\,(k_0-\Delta\,\mu)}}\;Im\,\Pi_N^{\alpha\beta} \;=\; -\,\frac{2}{1-e^{-\beta\,(k_0-\Delta\,\mu)}}\;Im\,\Pi_N^{R\alpha\beta} \quad . \tag{2.13}$$

Here $\Delta\mu = \mu_{out} - \mu_{in}$ is the difference of the chemical potentials between the outgoing and incident nucleons. Thus what we have to do is to somehow calculate Eqs. (2.11) or (2.12).

A. Thermodynamic Consistency

In this section, we discuss the thermodynamic consistency of the approximation for reaction rates with that for EOS. By consistency we mean the following: The reaction rates are nothing but correlation functions as stated above. For example, the density correlation function reduces in the static and long wave length to $\langle (N-\langle N\rangle)\cdot(N-\langle N\rangle)\rangle\,/\,V^2 = (\langle N^2\rangle - \langle N\rangle^2)\,/\,V^2$. Here N and V are the baryonic number and the volume of the system, respectively. This thermal ensemble average is related to the thermodynamic derivative of the number density with respect to the chemical potential as $(\partial N/\partial\mu)_T = \beta\,\langle (N-\langle N\rangle)\cdot(N-\langle N\rangle)$ with $\beta = 1/T$, which is obtained from EOS [39]. This sort of relation should be satisfied also in approximate formulations, since it guarantees the correct behavior of reaction rates in this limit. In the following we show that RPA is consistent in this sense with the mean field theory [18]. The argument is mainly indebted to the papers [40,41]. For simplicity we consider the non-relativistic density correlation in the imaginary time formalism. The extension to the relativistic case [42] and/or to the real time formalism is possible [43].

EOS can be calculated once the number density is obtained for a given temperature and chemical potential. The number density in turn is obtained from the single particle Green function as $n_b(x_1) = -i\,G(1,1^+)$. Here the Green function is defined as usual, $i\,G(1,2) = \langle T\,\phi(x_1)\phi^\dagger(x_2)\rangle$, and 1^+ in the argument denotes the limit $t_2 \to t_1 + 0$. Hence the approximation for EOS can be regarded as the approximation of the Green function, or that of the self energy Σ since the Green function is determined by the Dyson equation $G^{-1} = G_0^{-1} - \Sigma$, where G_0 is the free propagator.

The response of the system to the external disturbance is studied by adding the extra interaction like, $\mathcal{L}_{ext} = \int_0^{-i\beta} d\boldsymbol{x_1} dt_1 d\boldsymbol{x_2} dt_2\,\phi^\dagger(\boldsymbol{x_2},t_2)\,U(\boldsymbol{x_2},t_2,\boldsymbol{x_1},t_1)\,\phi(\boldsymbol{x_1},t_1)$, where only the time integration region is shown explicitly. Then the response function is given by

$$\left.\frac{\delta G(1,1';U)}{\delta U(2',2)}\right|_{U=0} \;=\; -\;\left[G_2(1,1',2,2') - G(1,1')\,G(2,2')\right] \;=\; i\,L(1,1',2,2') \quad , \tag{2.14}$$

where $G_2(1,1',2,2')$ is the two particle Green function, and $G(1,2;U)$ is the single particle Green function under the external disturbance and is written in the interaction representation as

$$i\,G(1,2;U) \;=\; \frac{\langle T\;S\,\phi(x_1)\,\phi^\dagger(x_2)\rangle}{\langle T\;S\rangle} \tag{2.15}$$

with $S = \exp(-i\mathcal{L}_{ext})$. Eq. (2.14) is derived directly by taking a derivative of Eq. (2.15). The retarded Green function defined by Eq. (2.12) is obtained from the response function $L(1,1^+,2,2^+)$ by the analytic continuation [39]. The equation for the response function $L(1,1',2,2')$ is obtained by taking a functional derivative of the Dyson equation as

$$L(1,1',2,2') \;=\; L_0(1,1',2,2') \;-\; \int dx_3 dx_{3'} dx_4 dx_{4'}\;L_0(1,1',3,3')\cdot\Xi(3',3,4',4)\cdot L(4,4',2,2') \tag{2.16}$$

with

$$i\,L_0(1,1',2,2') \;=\; G(1,2')\,G(2,1') \tag{2.17}$$

$$i\,\Xi(1',1,2',2) \;=\; \frac{\delta\Sigma(1',1)}{\delta G(2,2')} \quad . \tag{2.18}$$

It was shown [41] that if the self-energy Σ is derived from a potential as $\Sigma(1',1) = \delta\Phi/\delta G(1,1')$, or the integrability condition $\delta\Sigma(1',1)/\delta G(2,2') = \delta\Sigma(2',2)/\delta G(1,1')$ is satisfied, then the approximation is conservative, that is, the approximate number density as well as the response function so obtained satisfies the conservation equation just like the exact one. This result in turn dictates the behavior of the response function in the static and long wave length limit as follows. The response function is in general given by

$$L(\Omega,\boldsymbol{k}) \;=\; \frac{1}{2\pi}\int_{-\infty}^{\infty} dk_0\;\frac{L^{>}(k_0,\boldsymbol{k})-L^{<}(k_0,\boldsymbol{k})}{\Omega-k_0} \;=\; \frac{1}{2\pi}\int_{-\infty}^{\infty} dk_0\;\frac{(1-e^{-\beta k_0})\,L^{>}(k_0,\boldsymbol{k})}{\Omega-k_0} \quad . \tag{2.19}$$

Here $L(\Omega,\boldsymbol{k})$ is a Fourier transform of $L(1,1^+,2,2^+)$ with respect to x_1-x_2 and Ω is an imaginary energy. $L^{>}(k_0,\boldsymbol{k})$ and $L^{<}(k_0,\boldsymbol{k})$ are analytic functions with respect to k_0 and are Fourier transformed from $L^{>}(x_1,x_2)=\langle(n_b(x_1)-\langle n_b(x_1)\rangle)\cdot(n_b(x_2)-\langle n_b(x_2)\rangle)\rangle$ and $L^{<}(x_1,x_2)=\langle(n_b(x_2)-\langle n_b(x_2)\rangle)\cdot(n_b(x_1)-\langle n_b(x_1)\rangle)\rangle$, respectively. Thus $L^{>}(x_1,x_2)$ is nothing but a density correlation function we are seeking for. In fact, we use this equation (2.19) to derive the density correlation function $L(\Omega,\boldsymbol{k})$. If the approximate response function satisfies the conservation law, $L^{>}(k_0,0)=2\pi\,\delta(k_0)\,\tilde{L}^{>}(0,0)$ in the long wave length limit, $|\boldsymbol{k}|\to 0$. This then results in the equation

$$\lim_{|\boldsymbol{k}|\to 0} L(0,\boldsymbol{k}) \;=\; -\,\beta\,\tilde{L}^{>}(0,0) \;=\; -\,\beta\,V\,\langle(n_b-\langle n_b\rangle)\cdot(n_b-\langle n_b\rangle)\rangle \quad . \tag{2.20}$$

On the other hand, the thermodynamical derivative, $(\partial n_b/\partial\mu)_T=-i\,\partial G(1,1^+)/\partial\mu$, is evaluated from the Dyson equation as

$$\begin{aligned}
\frac{\partial G(1,1')}{\partial\mu} \;&=\; -\int dx_2 dx_{2'}\; G(1,2')\cdot\frac{\partial G^{-1}(2',2)}{\partial\mu}\cdot G(2,1') \\
&=\; -\int dx_2 dx_{2'}\; G(1,2')\,\left[\delta(2'-2)-\frac{\partial\Sigma(2',2)}{\partial\mu}\right]\,G(2,1') \\
&=\; -\int dx_{2'}\; G(1,2')\cdot G(2',1') \\
&\quad +\int dx_2 dx_{2'} dx_3 dx_{3'}\; G(1,2')\cdot i\,\Xi(2',2,3',3)\cdot G(2,1')\cdot\frac{\partial G(3,3')}{\partial\mu}.
\end{aligned} \tag{2.21}$$

Solving this equation using Eqs. (2.16), (2.20), we get

$$\left(\frac{\partial N}{\partial\mu}\right)_T \;=\; -\,i\,V\,\frac{\partial G(1,1^+)}{\partial\mu} \;=\; V\lim_{|\boldsymbol{k}|\to 0} L(0,\boldsymbol{k}) \;=\; \beta\,\langle(N-\langle N\rangle)(N-\langle N\rangle)\rangle \quad . \tag{2.22}$$

This is the equation which represents the thermodynamical consistency between the response function and EOS. So far the only assumption is that we have used the same approximate self energy for EOS and the response function. Hence the above argument can be applied to any conserved current and conserving approximation. In the next section, we consider a specific approximation of the self energy which leads to the mean field theory and RPA.

B. RPA

We base our discussion on the Lagrangian of the relativistic mean field (RMF) theory:

$$\begin{aligned}
\mathcal{L}_{RMF} \;&=\; \overline{\psi}_N\,(\,i\,\gamma_\mu\,\partial^\mu \;-\; M_N \;-\; g_\sigma\,\sigma \;-\; g_\omega\,\gamma_\mu\,\omega^\mu \;-\; g_\rho\,\gamma_\mu\,\tau^a\,\rho^{a\mu}\,)\,\psi_N \\
&+\; \frac{1}{2}\,\partial_\mu\,\sigma\,\partial^\mu\,\sigma \;-\; \frac{1}{2}\,m_\sigma^2\,\sigma^2 \;-\; \frac{1}{3}\,g_2\,\sigma^3 \;-\; \frac{1}{4}\,g_3\,\sigma^4 \\
&-\; \frac{1}{4}\,F_{\mu\nu}\,F^{\mu\nu} \;+\; \frac{1}{2}\,m_\omega^2\,\omega_\mu\,\omega^\mu \;+\; \frac{1}{4}\,c_3\,(\omega_\mu\,\omega^\mu)^2 \\
&-\; \frac{1}{4}\,G^a_{\mu\nu}\,G^{a\mu\nu} \;+\; \frac{1}{2}\,m_\rho^2\,\rho^a_\mu\,\rho^{a\mu} \quad ,
\end{aligned} \tag{2.23}$$

where the standard notations are used: ψ_N denotes a baryonic field of mass M_N. σ, ω_μ and ρ^a_μ are σ, ω and ρ meson fields with $m_\sigma=511$MeV, $m_\omega=783$MeV and $m_\rho=770$MeV, respectively. $F_{\mu\nu}$ and $G^a_{\mu\nu}$ are the antisymmetric field tensors for ω and ρ mesons. The constants $g_\sigma=10.0$, $g_\omega=12.6$ and $g_\rho=4.6$ are the coupling constants for the interactions between mesons and nucleons. $g_2=-7.2\mathrm{fm}^{-1}$, $g_3=0.62$ and $c_3=71.3$ are the self-coupling constants for σ and ω mesons. The quoted numbers are taken from the TM1 parameter set published by Sugahara & Toki [31](see also [30]).

The approximate self-energy employed in the mean field theory is given as follows. For simplicity, only the contribution from σ meson, that is the scalar part, is shown. The extension to other meson contributions is done in an analogous way.

$$\Sigma_s(1',1) \;=\; g_\sigma\,\delta(1-1')\cdot\sigma(1) \quad , \tag{2.24}$$

where σ meson is assumed to be a classical field and obeys the equation of motion:

$$(\partial_\nu\partial^\nu \;+\; m_\sigma^2)\,\sigma \;+\; g_2\,\sigma^2 \;+\; g_3\,\sigma^3 \;=\; -\,\Delta_0^{-1}\,\sigma \;+\; g_2\,\sigma^2 \;+\; g_3\,\sigma^3 \;=\; -\,g_\sigma\langle\,\overline{\psi}_N\psi_N\,\rangle \quad . \tag{2.25}$$

Here Δ_0^{-1} is the inverse of the free propagator. Solving Eqs. (2.24), (2.25) with the Dyson equation of nucleon consistently for stationary and uniform matter, we obtain RMF for the nuclear EOS.

On the other hand, using the same self-energy and Eq. (2.25), we can evaluate Ξ defined by Eq. (2.18) as

$$\Xi(1',1,2',2) \;=\; g_\sigma^2\,\delta(1'-1)\,\delta(2'-2)\cdot\left[-\,\Delta_0^{-1}(1-2) \;+\; 2\,g_2\,\overline{\sigma} \;+\; 3\,g_3\,\overline{\sigma}^2\right]^{-1}\,\delta(1-2) \quad , \tag{2.26}$$

where $\overline{\sigma}$ is the expectation value of σ in the static uniform matter. It is obvious that this approximation is conserving in the above sense. Putting this into Eq. (2.16), we get the equation for $L(1,1^+,2,2^+)$ as

$$L(1,1^+,2,2^+) \;=\; L_0(1,1^+,2,2^+) \;-\; \int dx_3dx_4\; L_0(1,1^+,3,3^+)\cdot\frac{-\,g_\sigma^2}{\tilde{\Delta}^{-1}(3-4)}\cdot L(4,4^+,2,2^+) \quad . \tag{2.27}$$

Here $\tilde{\Delta}^{-1} \;=\; \Delta_0^{-1} \;-\; 2\,g_2\,\overline{\sigma} \;-\; 3\,g_3\,\overline{\sigma}^2$. This is well known RPA except for the modification of the meson propagator due to its self-coupling. Thus we established the thermodynamic consistency between RMF and RPA.

It should be noted that the modified meson propagator is also obtained by expanding the Lagrangian around the stationary point up to the quadratic order of perturbation [44–47]. Since the stationary solution is nothing but the mean field, the correlation is described by the harmonic oscillation around the mean field in the above approximation. In this sense, it is natural that we get RPA consistent with RMF in the static and long wave length limit.

The above argument is in a rigorous sense applicable only to the conserved quantity such as the baryonic number. In general the axial vector part of the nucleon weak current is not a conserved current. However, we extend the above method to the axial vector contribution, since we can thus argue both vector and axial vector contributions on the same basis. Moreover, the interpretation that we describe the correlations by the harmonic oscillations around the static and uniform mean field is still valid. Thus the basic equations of RPA are summarized as

$$\begin{aligned} Tr\left[\,\Gamma^a\,L(1-2)\,\Gamma^b\,\right] \;&=\; Tr\left[\,\Gamma^a\,L_0(1-2)\,\Gamma^b\,\right] \\ &-\; \int dx_3dx_4\sum_{\Gamma^c} Tr[\,\Gamma^a\,L_0(1-3)\,\Gamma^c\,]\cdot V_{pot}^c(3-4)\cdot Tr\left[\,\Gamma^c\,L(4-2)\,\Gamma^b\,\right] \quad . \end{aligned} \tag{2.28}$$

Here $L(1-2)$ and $L_0(1-2)$ are the abbreviations of $L(1,1^+,2,2^+)$ and $L_0(1,1^+,2,2^+)$, respectively. Γ's denote gamma matrices, $\mathbf{1},\gamma^\mu,\gamma^\mu\gamma_5$, and the matrix structure of the response functions is explicitly indicated by the trace operations. V_{pot} is the nuclear potential mediated by mesons and is given by the modified propagators as

$$V_{pot}^s(1-2) \;=\; -\,g_\sigma^2\,\tilde{\Delta}(1-2) \tag{2.29}$$

for σ meson, for example. The response function $L(1-2)$ is analytically continued to the retarded Green function, which in turn gives the structure functions by Eq. (2.13). It is also possible to work in the real time formalism from the beginning, which we did in this paper. Regardless, they are equivalent to each other [48]. The explicit expressions of $Tr[\,\Gamma^a\,L_0(1-3)\,\Gamma^c\,]$ are given in Appendix.

It is clear from the above derivation that RPA is an approximation obtained from the self-energy evaluated up to the first order of the coupling constant and that processes such as collisions of nucleons are ignored. This can be understood from the fact that RPA is also obtained from the collisionless Boltzmann equation [39]. The collisional effect might be important particularly in the low density regime [24,25,27] and could in principle be included in the present formulation by taking higher order corrections of the self-energy [49]. It is, however, very difficult to do this in practice. In this paper we make more of the consistency of the approximations used for reaction rates and EOS we have currently at hand. The study of possible effects of scatterings which was discussed in the introduction will be published elsewhere [36].

In RMF we ignore the negative energy contribution to the nucleon spinor. In so doing, the positive energy part is defined in a density-dependent way. This extra density dependence should have made Eqs. (2.27), (2.28) more complicated, which we ignored in this paper. It should be noted that this inconsistency is quite minor except for small parametr regions very close to the phase boundary with which we are not concerned here.

C. Residual Interactions

The Lagrangian shown above does not include the contributions of the pion and the tensor coupling of the ρ meson since they do not contribute to the mean field [30,31]. To describe fluctuations in spin and isospin around the mean field these residual interactions should be added to the above Lagrangian as [50]

$$\mathcal{L}_{res} \;=\; \mathcal{L}_\pi \,+\, \mathcal{L}_\rho \;=\; -\,\overline{\psi}_N \left[i\,\frac{g_\pi}{2M_N}\,\gamma^\mu\,\gamma_5\,\partial_\mu \pi^a \;-\; \frac{g_\rho\,C_\rho}{2M_N}\,\sigma_{\mu\nu}\,\partial^\nu \rho^{a\mu} \right] \tau^a\,\psi_N \tag{2.30}$$

with $g_\pi^2/4\pi = 14.08$, $g_\rho^2/4\pi = 0.41$ and $C_\rho = 6.1$. Accordingly $\sigma^{\mu\nu}$ is added to Γ's in Eq. (2.28).

It is also known that there are short ranged repulsive correlations for these isovector channels. They are conveniently included by the phenomenological Landau – Migdal parameters [32]. In this paper they are implemented, following Horowitz & Piekarewicz [34,57], by modifying the meson propagators as

$$\frac{1}{q_\mu^2 \,-\, m_\pi^2} \;\rightarrow\; \left[\frac{1}{q_\mu^2 \,-\, m_\pi^2} \;-\; \frac{g'_\pi}{q_\mu^2} \right] \tag{2.31}$$

$$\frac{1}{q_\mu^2 \,-\, m_\rho^2} \;\rightarrow\; \left[\frac{1}{q_\mu^2 \,-\, m_\rho^2} \;-\; \frac{g'_\rho}{q_\mu^2} \right] \tag{2.32}$$

with the Landau – Migdal parameters $g'_\pi = 0.70$ and $g'_\rho = 0.30$. Unlike the conventional non-relativistic treatment, we take different parameter value for ρ mesons from pions, which better reproduces the electron scattering data as well as the spin-transfer observables in (p,n) reactions [34,35,51–53,57].

As for the electromagnetic interaction, we make the Thomas-Fermi approximation, where the photon propagator is replaced by the screened one as

$$\frac{g_{\mu\nu}}{-\,q_\mu^2} \qquad \rightarrow \qquad \frac{g_{\mu\nu}}{q_{TF}^2 \,-\, q_\mu^2} \tag{2.33}$$

with $q_{TF}^2 = 4\,e^2\,\pi^{1/3}(3\,n_e)^{2/3}$, where e and n_e are the electron charge and number density, respectively. Then it was added to the V_{pot}'s in Eq. (2.28).

It is finally noted that since the neutrino couples only to the spin-transverse correlations in RPA, the pion (spin-longitudinal correlations) does not contribute to the neutrino reaction rates considered here.

III. RESULTS

A. Neutral Current Reactions

In this section, we discuss correlation effects on the neutral current reactions, that is, neutrino – nucleon scatterings. The high density regime, $\rho_b \geq 2\times10^{14}$g/cm^3, and the low density regime, $\rho_b < 2\times10^{14}$g/cm^3, are discussed separately, since the behaviors of $R_1(k)$ in Eq. (2.8), which is refered to as the vector current correlations in the following, are qualitatively different between the two regimes.

The vector current correlation is mainly induced by the scalar isoscalar meson σ and the vector isoscalar meson ω, while the axial vector current, which is more important for the neutrino opacity, is dominantly affected by the vector isovector meson ρ.

As shown shortly, the structure functions of nucleons are in general narrow peaked as a function of the transferred energy in the sense that their width is much smaller than the transferred three momentum. This feature reflects the fact that the nucleon mass is typically much greater than the neutrino energy and the scattering is almost isoenergetic. If we assume that the scatterings are exactly isoenergetic, that is, the structure functions are proportional to the delta function of the transferred energy, then we obtain the well known Bruenn's formula [2] which we use as a reference in this paper. In some cases this approximation alone overestimates the cross section significantly [54]. This issue will be addressed again in the following sections.

1. high density regime

First we consider the high density regime, $\rho_b \geq 2 \times 10^{14}\mathrm{g/cm}^3$. Fig. 1 shows the structure functions $R_1(k_0, |\overrightarrow{\boldsymbol{k}}|)$ and $R_2(k_0, |\overrightarrow{\boldsymbol{k}}|)$ as a function of the transferred energy k_0 for the density, temperature and proton fraction given in the figure. The transferred three momentum $|\overrightarrow{\boldsymbol{k}}|$ is taken to be a typical neutrino energy $\sim 3\,T$. The long dashed curves correspond to the structure functions of the non-interacting nucleons. The width of the structure functions gives a measure of average energy exchange between neutrino and nucleon. As stated above, we obtain the Bruenn's formula [2] if we neglect this width of these functions entirely and approximate the structure functions by the delta functions of k_0 as:

$$R_1(k_0, |\overrightarrow{\boldsymbol{k}}|) \approx 2\,\pi\,\delta(k_0)\,\cdot\,\left[\,{h_V^n}^2\,\eta_n\,+\,{h_V^p}^2\,\eta_p\,\right] \tag{3.1}$$

$$R_2(k_0, |\overrightarrow{\boldsymbol{k}}|) \approx 2\,\pi\,\delta(k_0)\,\cdot\,\left[\,{h_A^n}^2\,\eta_n\,+\,{h_A^p}^2\,\eta_p\,\right] \tag{3.2}$$

with $\eta_N = \displaystyle\int \frac{2\,d^3p}{(2\pi)^3}\,f_N(p)[1-f_N(p)]$ for $N = n, p$. Here $f_N(p)$ is Fermi-Dirac distribution function for the nucleon. Note that the long wave length limit $|\overrightarrow{\boldsymbol{k}}| \to 0$ is also taken in this approximation. It is obvious from the figure that this approximation is not very good for this large momentum transfer which is common in the hot proto neutron star [54]. It should be noted that the neglection of the energy transfer leads to the overestimation of the reaction rate.

The short dashed curves are obtained from the first term including L_0 on the right hand side of Eq. (2.28), where only the modified dispersion relation in medium, that is, the effective mass and potential of nucleons is taken into account. Note the effective mass of the nucleon becomes as small as $\sim 0.6M_N$ in RMF (see [30,31]). The low effective mass renders the structure functions a little bit wider than for the non-interacting case, since the energy exchange between neutrino and nucleon is more facilitated, and lowers their amplitudes as well. It is important to note that with this modification alone, the neutrino scattering rates are considerably reduced [3]. However, as shown in the preceding section, the inclusion of the effective mass alone is not consistent with EOS obtained in RMF.

The solid curves in the figure shows the structure functions with the RPA correlation. As already mentioned, the scalar isoscalar meson σ and the vector isoscalar meson ω are the dominant agents of the correlation for $R_1(k)$. In the high density regime, the contribution of ω dominates over that of σ, making the nuclear force effectively repulsive and having the structure function even smaller for small k_0. On the other hand, the ρ meson is the dominant mediator of the nuclear correlation for $R_2(k)$. Since the typical transferred momentum is still small enough for the short ranged repulsive force described by the Landau – Migdal parameters to be dominant, the response of this channel is also suppressed. The feature mentioned here is common to the structure functions in this density regime.

As the temperature decreases, the structure function is more skewed toward the positive energy transfer $k_0 > 0$, reflecting the fact that the extraction of energy from the nuclear medium becomes more difficult due to the Fermi blocking for the down scattered nucleon. This is shown in Fig. 2.

On the other hand, as the density becomes higher, the nucleon effective mass gets smaller ($M_N^* \sim 0.4M_N$ at $\rho_b = 5 \times 10^{14}\mathrm{g/cm}^3$), making the amplitudes of the structure functions, both for $R_1(k)$ and $R_2(k)$, smaller without RPA. The ω meson becomes even more dominant over the σ meson and thus RPA further reduces the amplitude of $R_1(k)$, as shown in Fig. 3.

The case of the proton fraction $Y_p = 0.1$ is shown in Fig. 4. The effect of RPA increases with decreasing Y_p, which could be understood as follows. The vector current correlation comes mainly from the neutron sector, since the coupling constant for proton $h_V^p \sim 0$. Since the neutron density increases as the proton fraction decreases, the vector current correlation becomes greater, reducing the structure function $R_1(k)$.

The total scattering rate of the neutrino with the incident energy E_ν^{in} is given by the integration of the structure function with respect to the transferred momentum $\overrightarrow{\boldsymbol{k}}$ and energy k_0:

$$\begin{aligned} R^{tot}(E_\nu^{in}) &= \int \frac{d^3q_\nu^{out}}{(2\pi)^3}\,\frac{1}{2E_\nu^{in}\,2E_\nu^{out}}\;R(E_\nu^{in},\,E_\nu^{out},\,\cos\theta)\;\left[\,1\,-\,f_\nu(E_\nu^{out})\,\right] \\ &= \frac{1}{(2\pi)^3}\,\int_0^\infty 2\pi k\,dk\,\int_{-k}^{k_0^{max}} dk_0\;\frac{E_\nu^{in}-k_0}{E_\nu^{in}}\,\frac{1}{2E_\nu^{in}\,2E_\nu^{out}}\;R(E_\nu^{in},\,E_\nu^{out},\,\cos\theta)\;\left[\,1\,-\,f_\nu(E_\nu^{out})\,\right], \end{aligned} \tag{3.3}$$

with $k_0^{max} = min(k,\,2E_\nu^{in}-k)$. If we ignore the energy exchange and the Fermi blocking for the scattered neutrino, and insert Eqs. (3.1) and (3.2) into R_1 and R_2 in the above equation, we obtain the standard approximate formula [2]

$$R^{tot}(E_\nu^{in}) \;\approx\; \sum_{N=n,p}\,\frac{G_F^2}{\pi}\;\left(E_\nu^{in}\right)^2\;\left\{\,\eta_N\,\left[\,\left(h_V^N\right)^2\,+\,3\,\left(h_A^N\right)^2\,\right]\,\right\} \tag{3.4}$$

which is frequently used in literatures. In the following we use this rate as a reference in evaluating quantitatively the suppression factors of the total scattering rates due to the correlation. It should be noted, however, that the difference between these rates also comes from the inclusion of the effective nucleon mass and the finite energy and momentum transfer, which are neglected in Eq. (3.4).

Fig. 5 shows the ratio of R^{tot} evaluated for the first term in Eq. (2.28) by using the exact formula given in Eq. (3.3) to R^{tot} by using the approximate expression given in Eq. (3.4) as a contour map in the density and temperature plane for the given proton fraction. The contributions from R_1 and R_2 are shown separately. The incident neutrino energy is assumed to be $3\,T$, and the blocking factor was dropped again.

It is again clear that the reaction rates are substantially smaller than the standard ones before RPA is included. This is mainly due to the decrease of the nucleon effective mass. In fact, as the density increases, the reduction becomes greater, which is common to the vector current part from R_1 and the axial vector current part from R_2. The non-monotonic temperature dependence is understood as follows: In the standard approximation formula, as mentioned above, the energy exchange between neutrino and nucleon is neglected. In the low temperature regime, this neglection tends to overestimate the Fermi blocking for the scattered nucleon, reducing the standard rate. As a result, the suppression factor becomes larger as the temperature increases. For even higher temperature, however, the width of the structure function cannot be ignored and lowers the total scattering rate just like the neutrino – electron scattering. Since the latter effect surpasses the former at some temperature, the suppression factor begins to decrease again above this temperature, which becomes larger as the density increases. These features were discussed in the paper by Schinder [54] where he studied the effect of the recoil of nucleons.

Fig. 6 shows the suppression factor for the reaction rates with the inclusion of RPA. It is evident that both the vector current and axial vector current contributions are further suppressed, which is expected from the above results for the structure functions. Indeed the reaction rates become less than half the standard rates around the saturation density. Since the delayed explosion is very sensitive to the neutrino luminosity and the energy, this suppression could have an significant influence on the final outcome of the core collapse.

we can understand the different density and temperature dependences of the vector and axial vector contributions. In the former case, the RPA suppression is strongly density dependent, since the nuclear force is determined by the competition of the attractive σ meson and the repulsive ω meson. As a result, the reaction rates are more strongly suppressed in the higher density regime. On the other hand, the balance between the attractive ρ meson and the repulsive short range force described by the Landau – Migdal parameter is determined by the momentum transfer, thus more temperature dependent. Since the nuclear force is more repulsive for the smaller momentum transfer, that is, in the low temperature regime, the rate is reduced further there.

Figs. 7 and 8 shows the suppression factors for the different proton fractions. As expected, the axial vector part is more affected, since the isovector ρ meson is convening its correlation. It is also clear that the suppression is stronger for the smaller proton fraction.

2. low density regime

The low density regime considered here is characterized by the appearance of nuclei for low temperatures [28,29,55]. Although we cannot treat the coexistence phase of nuclei and nucleons by the current formulation and consider here only the gas phase where no nuclei exist, the precursor of the phase transition is already imprinted in this regime.

On the contrary to the previous section, the σ meson dominates the ω meson and the isoscalar nuclear force becomes attractive. As a result, the correlation enhances the reaction rate coming from the vector current part. This can be seen in Fig. 9, where the structure functions R_1 and R_2 are shown for the temperature near the phase boundary. The enhancement of R_1 in the vicinity of $k_0 = 0$ suggests the existence of the static unstable mode [56]. In fact, R_1 diverges on the so-called spinodal line [57]. From the thermodynamic consistency discussed above, $\left(\frac{\partial N}{\partial \mu}\right)_T$ also diverges on this line. This behavior is better indicated in Fig. 10, in which the enhancement factor with respect to the standard Bruenn's formula is plotted as a contour in the density temperature plane. As the temperature decreases, the reaction rate becomes larger. The lower boundary of the computation region roughly corresponds to the spinodal line obtained by the current model. Incidentally, the axial vector contribution is hardly affected since the σ and ω mesons are minor contributors for this channel.

Since in reality this liquid-gas phase transition occurs not by the spinodal decomposition but by the nucleation, the actual phase boundary does not correspond to the spinodal line except for the critical point, and the spinodal line is never reached [28,29,55]. The critical temperature obtained from RPA is about 15MeV, which is actually consistent with the value obtained from EOS by Shen et al. [28,29].

Although the enhancement factor is still relatively large in the region not very close to the phase boundary, this effect has only minor importance for the neutrino opacity, because the vector current contribution is typically much

smaller ($\sim 1/4$) than the axial vector contribution. Provided that the axial vector part is slightly suppressed in this regime due to the repulsive nuclear interaction for that channel, the total scattering rate will not be increased significantly unless the critical point is approached very closely.

B. Charged Current Reactions

The RPA correlation is calculated for the charged current reactions just the same way as for the neutral current reactions except that the vector isovector ρ meson is the only mediator of the correlation. It is noted again that since only the spin-transverse correlation matters for the neutrino reaction rates in RPA, the pion does not make any contribution. As a result, for relatively small momentum transfer of our current interest the nuclear force is repulsive and the correlation always tends to suppress both the vector current and the axial vector current contribution to the charged current reaction rates like the axial vector part of the neutral current. This is true not only for the high density regime but also for the low density regime unlike the vector current part of the neutral current reaction rates which is enhanced by the liquid – gas phase transition.

Fig. 11 shows a typical modification of the structure functions around the saturation density for the symmetric nuclear matter. Depicted are $R_1(k_0, |\overrightarrow{\boldsymbol{k}}|)$ and $R_2(k_0, |\overrightarrow{\boldsymbol{k}}|)$ for the $e^- + p \to \nu_e + n$ reaction with the outgoing neutrino energy of $\sim \mu_e$, the electron chemical potential. It is clear again that the decrease of the nucleon effective mass alone (the short dashed curve) accounts for more than half of the suppression with respect to the non-interacting case (the long dashed curve). Moreover, as the electron chemical potential is quite large, ~ 250MeV, the average energy transfer from the incident electron to the nucleon becomes also large. Hence the complete neglection of energy transfer assumed in the approximate formula [2] leads to sizable overestimation of the reaction rates for this high energy neutrino emission.

The results change qualitatively for the asymmetric matter, since the potential for the neutron is different from that for the proton in medium. This is understood as follows. In the non-relativistic limit the dispersion relation for the nucleon is written as

$$E_N(\overrightarrow{\boldsymbol{k}}) \;=\; \frac{|\overrightarrow{\boldsymbol{k}}|^2}{2M_N^*} \,+\, U_N^{pot} \quad , \tag{3.5}$$

and the potential difference is given in RMF by

$$\Delta U_{pn}^{pot} \;\equiv\; U_p^{pot} \,-\, U_n^{pot} \;=\; 2\, g_\rho \langle \rho \rangle \;=\; 2\, \frac{g_\rho^2}{m_\rho^2}\, (n_p - n_n) \quad . \tag{3.6}$$

Thus, in neutron rich matter, the proton is more strongly bound than the neutron. This difference of potentials serves as a threshold for the $p \to n$ reaction as the mass difference of nucleons does for the reaction in vacuum. It is, however, ignored in the approximate formula [2], which is given by

$$R_1(k_0,\, |\overrightarrow{\boldsymbol{k}}|) \approx 2\,\pi\,\delta(k_0 - \Delta)\,\cdot\, {g_V}^2\;\eta_{pn} \tag{3.7}$$

$$R_2(k_0,\, |\overrightarrow{\boldsymbol{k}}|) \approx 2\,\pi\,\delta(k_0 - \Delta)\,\cdot\, {g_A}^2\;\eta_{pn} \tag{3.8}$$

with $\eta_{pn} = \displaystyle\int \frac{2\,d^3p}{(2\pi)^3}\, f_p(p)[1 - f_n(p)]$. Hence the structure functions in this approximation are delta functions placed at $k_0 = \Delta \equiv M_n - M_p$.

With the potential difference taken into account, however, the structure functions are shifted by $-\Delta U_{pn}^{pot}$, thus they do not agree with the approximate ones even in the static and long wave length limit with $M_N^* \to M_N$. This is seen in Fig. 12, where the structure functions for the asymmetric matter ($Y_p = 0.3$) are shown for the non-interacting case (the long dashed curve) as well as the case with the nucleon effective mass and potential alone included (the short dashed curve) and the case with RPA also included (the solid curve). In the non-interacting case, the structure functions are located around $k_0 \sim \Delta$, while in the other cases they are moved toward the positive energy transfer as stated above.

The total ν_e emission rate is given for an outgoing neutrino energy E_ν^{out} as

$$\begin{aligned} R^{tot}(E_\nu^{out}) &= \int \frac{d^3q_e^{in}}{(2\pi)^3}\, \frac{1}{2E_e^{in}\, 2E_\nu^{out}}\; R(E_e^{in},\, E_\nu^{out},\, \cos\theta)\; f_e(E_e^{in}) \\ &= \frac{1}{(2\pi)^3}\, \int_0^\infty 2\pi k\, dk\, \int_{k_0^-}^{k_0^+} dk_0\; \frac{E_\nu^{out} + k_0}{E_\nu^{out}} \frac{1}{2E_e^{in}\, 2E_\nu^{out}}\; R(E_e^{in},\, E_\nu^{out},\, \cos\theta)\; f_e(E_e^{in}) \quad , \end{aligned} \tag{3.9}$$

where $k_0^{\pm} = \sqrt{m_e^2 + (E_\nu^{out} \pm k)^2} - E_\nu^{out}$. Inserting Eqs. (3.7), (3.8) into the above equation, we obtain the standard approximate formula:

$$R^{tot}(E_\nu^{out}) \;\approx\; \frac{G_F^2}{\pi}\,({g_V}^2 + 3\,{g_A}^2)\,\eta_{pn}\,(E_\nu^{out}+\Delta)^2\sqrt{1-\left(\frac{m_e}{E_\nu^{out}+\Delta}\right)^2}\,f_e(E_\nu^{out}+\Delta) \quad . \tag{3.10}$$

For the symmetric nuclear matter, the density and temperature dependence of the suppression factor of the total emission rates, that is the ratio of Eq. (3.9) to Eq. (3.10), is essentially the same as that of the axial vector contribution to the neutral current reaction. For the asymmetric matter, as understood from Eq. (3.9), the k integration has greater contribution from larger momentum transfer due to the shift of the structure functions, which tends to get the reaction rates larger thanks to the larger phase volume. However, as E_ν^{out} comes closer to μ_e, the electron population starts to deplete $f_e(E_e^{in}) \lesssim 1$ and, as a result the emission rate becomes smaller. This occurs for smaller E_ν^{out} in Eq. (3.9) than in Eq. (3.10) due to the large width of the structure function. It follows that the total emission rate is greater than the approximate one given by Eq. (3.10) for neutrinos with energy $E_\nu^{out} \ll \mu_e$ and smaller for neutrinos with $E_\nu^{out} \lesssim \mu_e$. This is indicated in Fig. 13. Thus lower energy electron neutrinos are produced more efficiently than predicted from the standard approximate formula. It is also seen that the RPA correction is not very large since the nuclear force becomes less repulsive for the large momentum transfer considered here.

Fig. 14 displays the structure functions for a lower temperature. It is evident that their widths became smaller. This is because nucleons become more degenerate as the temperature is lowered and the large energy transfer is required to overcome the difference of chemical potentials between neutron and proton. The comparison of Fig. 15, which represents the emission rates for the same temperature, with Fig. 13 shows that the emission of high energy neutrinos is severely suppressed for the low temperature, because it is contributed from the high energy tail of degenerate electrons. It is also seen from the figure that the approximate formula tends to overestimate the Fermi blocking factor for the outgoing neutron by neglecting the finite energy transfer, thus underestimating the emission rate. The RPA correction is even smaller in this case, since the narrow structure functions favor higher momentum transfer.

As the density is increased or the proton fraction is decreased, the potential difference becomes larger. Hence the features mentioned above become more prominent, which is demonstrated in Figs. 16 and 17. In the latter case, since the electron chemical potential is also decreased, it is possible for small Y_p and T that the structure functions and the electron distribution function in the integrand of Eq. (3.9) do not give a significant overlap and the emissivity is strongly reduced. This is well known suppression of the URCA process [58].

The structure functions for the $n \to p$ reactions are derived from those for the $p \to n$ reactions by using the detailed balance relation expressed as

$$R^{(n,\,p)}(k) \;=\; e^{\beta(k_0 - \Delta\mu_{pn})}\;R^{(p,\,n)}(-k) \quad , \tag{3.11}$$

where $\Delta\mu_{pn} = \mu_p - \mu_n$ is the difference of the nucleon chemical potentials. In this paper, however, the $n \to p$ structure functions were calculated in the same way as the $p \to n$ counterparts, and we confirmed directly that the above relation is actually satisfied.

As expected, the structure functions for the $n \to p$ reactions are shifted toward the negative energy transfer due to the potential difference for proton and neutron in asymmetric matter, which is shown in Fig. 18. The RPA correction accounts for about half of the total suppression in this case. The total emissivity of $\overline{\nu}_e$ via $e^+ + n \to \overline{\nu}_e + p$ is obtained from Eq. (3.9) with the following exchanges: $p \leftrightarrow n$, $e \leftrightarrow e^+$ and $\nu_e \leftrightarrow \overline{\nu}_e$. The important difference from the ν_e case comes from the fact that positrons are not degenerate in the supernova core. The shift of the structure functions in the direction of the negative energy transfer gives greater weights to positrons with lower energies which are more populated, leading to larger emissivity of $\overline{\nu}_e$. On the other hand, the RPA correction tends to reduce the rate as in the ν_e case. These trends are shown in Fig. 19, where the $\overline{\nu}_e$ emissivity is plotted as a function of the energy of the emitted neutrino. The potential difference for neutron and proton provides the emitted neutrino with certain energy ($\sim$ 30MeV in this case). Although the correlation reduces the emissivity substantially, the emissivity of high energy neutrinos are larger even after RPA is included than for the approximate formula.

Thus far, we discussed the ν emissivities. The corresponding absorption rates of ν_e via $\nu_e + n \to e + p$ and $\overline{\nu}_e$ via $\overline{\nu}_e + p \to e^+ + n$ are obtained by the detailed balance equation:

$$R_{ab}^{tot}(E_\nu) \;=\; e^{\beta(E_\nu - \mu_\nu)}\;R_{em}^{tot}(E_\nu), \tag{3.12}$$

where the neutrino chemical potential is defined as $\mu_{\nu_e} \equiv \mu_e + \mu_p - \mu_n$ for ν_e and $\mu_{\overline{\nu}_e} = -\mu_{\nu_e}$ for $\overline{\nu}_e$. This relation is easily proven from Eq. (3.11).

IV. CONCLUSION

In view of the application to supernova simulations [59,60], we have calculated the neutrino – nucleon reaction rates in hot and dense supernova cores with the RPA correlations taken into account. The approximations are based on the Lagrangian used in RMF for the nuclear EOS, where the nonlinear σ and ω meson terms are included. This ensures the thermodynamic consistency in the static and long wave length limit between the EOS we use in the supernova simulations and the vector current correlation of nucleons which gives partial contributions to the neutrino – nucleon scattering rates. The same method is extended to the axial vector current as well as to the isovector current correlations with the residual interactions added which are described by the tensor coupling of the ρ meson and the so-called Landau-Migdal parameters.

We have found that the neutral current reactions are suppressed substantially in the high density regime, $\rho \gtrsim 10^{14}\mathrm{g/cm}^3$, due to the repulsive nature of the nuclear forces. In the lower density regime, however, the vector current contributions are enhanced as the temperature is decreased and the boundary of the gas phase, which is placed by RPA consistently with EOS, is approached. Although this is interesting itself, the total scattering rates are not enhanced significantly except for the very vicinity of the critical point, since the axial vector contribution is dominant over the vector current one and is unaffected by the liquid – gas phase transition. We have also shown that the neglection of the finite energy exchange between neutrino and nucleon, which is assumed in the standard approximation formula, can lead to a significant overestimation of the total reaction rates in the high temperature regime where the typical incident neutrino energy is no longer much smaller than the nucleon effective mass.

In the case of the charged current reactions, it is more important to take proper account of the potential difference for neutron and proton than to consider the RPA correlation, since it serves as a threshold of the reaction just as a mass difference does in vacuum. In fact, with the potential difference included the ν_e emissivity via $e + p \to \nu_e + n$ is much smaller for higher energy neutrinos than expected from the standard formula. On the other hand, the emission of low energy antineutrinos via $e^+ + n \to \overline{\nu}_e + p$ is reduced. In both cases, the RPA correlation reduces the total rates further.

These modifications of the neutrino – nucleon reaction rates could have an important impact on the mechanism of collapse-driven supernovae, since they are the dominant opacity sources for neutrinos. The smaller opacity leads to the larger neutrino luminosity, hence to the greater heating rate behind the stagnated shock wave, which gives a better odds to get a successful explosion. The changes of neutrino mean free paths, on the other hand, could also affect the strength and region of convections in the proto neutron star, which is one of the key ingredients to determine the neutrino luminosity and energy. These issues will be discussed in detail elsewhere [61].

It is clear that RPA does not include everything. As understood from the fact that RPA is consistent with the mean field theory for the equation of state, RPA studies the response of the mean field to the external disturbance. The additional correlations might be induced by some reactions such as collisions of two nucleons via spin and isospin dependent reactions, as pointed out by some authors. Although these effects can in principle be included in the above formulation by taking the corresponding higher order corrections to the self-energy, it is extremely difficult to achieve it in practice. In this paper we employed RPA respecting the consistency between the calculated reaction rates and EOS we have currently at our disposal. Nevertheless, these issues are remaining to be studied further.

ACKNOWLEDGMENTS

One of the authors (S.Y.) greatfully acknowledges critical discussions with H.-Th. Janka and G. Raffelt. He would highly appreciate various support by E. Müller during his stay in Max Planck Institut für Astrophysik. This work is partially supported by the Grants-in-Aid for the Center-of-Excellence (COE) Research of the Ministry of Education, Science, Sports and Culture of Japan to RESCEU (No.07CE2002).

APPENDIX: CAUSAL GREEN FUNCTIONS

Once the formulation is established in the imaginary time formalism, it is more convenient to work with quantities which are analytically continued from the imaginary time domian to the real time domain. Then Eq. (2.28) is still valid with the response functions replaced with the retarded Green functions. These real time retarded Green functions Eq. (2.12) are derived from the corresponding causal Green functions defined by Eq. (2.11) via the relation Eq. (2.13). Thus all we have to do is to calculate Π_N^{R0} and then to solve Eq. (2.28) which is now rewritten in momentum space as

$$\Pi_N^{R\,ab}(k) \;=\; \Pi_N^{R0\,ab}(k) \;-\; \sum_c \Pi_N^{R0\,ac}(k) \cdot V_{pot}^c(k) \cdot \Pi_N^{R\,cb}(k) \quad . \tag{A1}$$

Here $\Pi_N^{R0\,ab}(k)$ is derived by Eq. (2.13) from $\Pi_N^{0\,ab}(k)$ which is expressed as

$$i\,\Pi_N^{0\,ab}(k) \;=\; Tr\int\frac{d^4q}{(2\pi)^4}\,\Gamma^a\,G(q+k)\,\Gamma^b\,G(q) \quad , \tag{A2}$$

where Γ's stand for $\mathbf{1}, \gamma^\mu, \sigma^{\mu\nu}, \gamma^\mu\gamma_5$. $G(k)$ is a single particle Green function of nucleon given by RMF:

$$G(k) = G_F(k) \;+\; G_D(k) \tag{A3}$$

$$G_F(k) = \frac{\bar{\not{k}} + M_N^*}{\bar{k}^2 - {M_N^*}^2 + i\varepsilon} \tag{A4}$$

$$G_D(k) = (\bar{\not{k}} + M_N^*)\cdot 2\pi i\,\delta(\bar{k}^2 - {M_N^*}^2)\left\{\Theta(\bar{k}_0)\,f_N(k_0) \;+\; \Theta(-\bar{k}_0)\,f_{\bar{N}}(-k_0)\right\} \quad , \tag{A5}$$

where $\bar{k} = (k_0 - \Sigma_V, \boldsymbol{k})$, $M_N^* = M_N + \Sigma_S$ with Σ_S, Σ_V the sclar and vector nucleon self-energies given by RMF, and $f_N, f_{\bar{N}}$ are Fermi distribution functions for nucleon and antinucleon, respectively. Note that since the above Green function $G(k)$ already includes the effective mass and potential, $\Pi_N^0(k)$ is different from the response function of non-interacting nucleons. As shown in the above equation, the Green function is decomposed into two contributions, that is, the Feynman part $G_F(k)$ and the density-dependent part $G_D(k)$. As a usual practice, we ignore the vacuum polarization coming from the Feynman part alone in calculating $\Pi_N^0(k)$. Taking the proper linear combination of $\Pi_N^{R\,ab}$, we obtain the retarded Green function for the nucleon weak current, from which using again Eq. (2.13), we finally arrive at the structure functions of nucleons. The explicit expressions of Eq. (A2) are found, for example, in [22,23,62].

---

[1] D. L. Tubbs and D. N. Schramm, ApJ. **201**, 467 (1975)
[2] S. W. Bruenn, ApJS. **58**, 771 (1985)
[3] S. Reddy, M. Prakash and J. M. Lattimer, PRD. **58**, 013009 (1998)
[4] R. F. Sawyer, PRC. **40**, 865 (1989)
[5] N. Iwamoto and C. J. Pethick, PRD. **25**, 313 (1982)
[6] A. Burrows and J. M. Lattimer, ApJ. **307**, 178 (1986)
[7] A. Mezzacappa and S. W. Bruenn, ApJ. **405**, 637 (1993)
[8] A. Mezzacappa and S. W. Bruenn, ApJ. **405**, 669 (1993)
[9] A. Mezzacappa and S. W. Bruenn, ApJ. **410**, 740 (1993)
[10] H. Suzuki, Frontiers of Neutrino Astrophysics, Proc. of the International Symposium on Neutrino Astrophysics, Takayama/Kamioka, japan, Oct.19.-22., 1992, edited by Y. Suzuki and K. Nakamura, Universal Academy Press, Tokyo, 1993, p219
[11] H. -Th. Janka and E. Müller, Frontiers of Neutrino Astrophysics, Proc. of the International Symposium on Neutrino Astrophysics, Takayama/Kamioka, Japan, Oct.19.-22., 1992, edited by Y. Suzuki and K. Nakamura, Universal Academy Press, Tokyo, 1993, p203
[12] A. Burrows and J. Goshy, ApJ. **416**, 75 (1993)
[13] J. R. Wilson, Proc. Univ. Illinois Meeting on Numerical Astrophysics
[14] H. Bethe and J. R. Wilson, ApJ. **295**, 14 (1985)
[15] W. Keil, H. -Th. Janka and G. Raffelt, PRD. **51**, 6635 (1995)
[16] H. -Th. Janka, W. Keil, G. Raffelt and D. Seckel, PRL. **76**, 2621 (1996)
[17] S. Hannestad and G. Raffelt, ApJ. **507**, 339 (1998)
[18] A. Burrow and R. F. Sawyer, PRC. **58**, 554 (1998)
[19] A. Burrow and R. F. Sawyer, PRC. **59**, 510 (1999)
[20] S. Reddy, M. Prakash, J. M. Lattimer and J. A. Pons, astro-ph/9811294 (1998)
[21] H. Suzuki, Physics and Astrophysics of Neutrinos, edited by M. Fukugita and A. Suzuki, Springer-Verlag, Tokyo, 1994, p763
[22] S. Reddy, M. Prakash and J. M. Lattimer, Proc. Second Oak Ridge Symposium on Atomic and Nuclear Astrophysics, 1998
[23] C. J. Horowitz and K. Wehrberger, PLB. **266**, 236 (1991)
[24] G, Raffelt and D. Seckel, PRD. **52**, 1780 (1995)
[25] G, Raffelt, D. Seckel and G. Sigl, PRD. **54**, 2784 (1996)
[26] G, Raffelt and G. Sigl, sumitted PRD. (1998)
[27] R. F. Sawyer, PRL. **75**, 2260 (1995)

[28] H. Shen, H. Toki, K. Oyamatsu and K. Sumiyoshi, Nucl. Phys. A. **637**, 435 (1998)
[29] H. Shen, H. Toki, K. Oyamatsu and K. Sumiyoshi, Prog. Theor. Phys. **100**, 1013 (1998)
[30] K. Sumiyoshi and H. Toki, ApJ. **422**, 700 (1994)
[31] Y. Sugahara and H. Toki, Nucl. Phys. A. **579**, 557 (1994)
[32] A. B. Migdal, Rev. Mod. Phys. **50**, 107 (1978) and references therein
[33] C. J. Horowitz and J. Piekarewicz, PLB. **301**, 321 (1993)
[34] C. J. Horowitz and J. Piekarewicz, PRC. **50**, 2540 (1994)
[35] K. Yoshida and H. Toki, Nucl. Phys. A. **648**, 75 (1999)
[36] S. Yamada, in preparation, see also Proceedings of the 9th Workshops on Nuclear Astrophysics, Ringberg Castle, Tegernsee, Germany, Mar. 23.-27., 1998, editted by W. Hillebrandt and E. Müller, p115
[37] G. Raffelt, 'Stars as Laboratories for Fundamental Physics', University Chicago Press, Chicago, 1996
[38] N. P. landsman and Ch. G. van Weert, Phys. Rep. **145**, 141 (1987)
[39] L. P. Kadanoff and G. Baym, 'Quantum Statistical Mechanics', The Benjamin/Cummings Publishing Company, Inc., London, 1962
[40] G. Baym and L. P. Kadanoff, Phys. Rev. **124**, 287 (1961)
[41] G. Baym, Phys. Rev. **127**, 1391 (1962)
[42] B. Vanderheyden and G. Baym, J. Stat. Phys. in press
[43] Yu. B. Ivanov, J. Knoll and D. N. Voskresensky, submitted to Nucl. Phys. B. (1998)
[44] M. L'Huillier and Nguyen Van Giai, PRC. **39**, 2022 (1989)
[45] Z. Ma, Nguyen Van Giai, H. Toki and M. L'Huillier, PRC. **55** 2385 (1997)
[46] Z. Ma, H. Toki and Nguyen Van Giai, Nucl. Phys. A. **627**, 1 (1997)
[47] Z. Ma, H. Toki, B. Chen and Nguyen Van Giai, Prog. Theor. Phys. **98**, 917 (1997)
[48] F. Guerin, Nucl. Phys. B. **432**, 281 (1994)
[49] W. -D. Kraeft, D. Kremp, W. Ebeling and G. Röpke, 'Quantum Statistics of Charged Particle Systems', Akademieverlag, Berlin, 1986
[50] R. Brockmann and R. Machleidt, PRC. **42**, 1965 (1990)
[51] P. Barreau et al., Nucl. Phys. A. **402**, 515 (1983)
[52] X. Y. Chen et al., PRC. **47**, 2159 (1993)
[53] H. Sakai et al., Nucl. Phys. A. **577**, 111 (1994)
[54] P. J. Schinder, ApJS. **74**, 249 (1990)
[55] H. Müller and B. D. Serot, PRC. **52**, 2072 (1995)
[56] K. Lim and C. J. Horowitz, Nucl. Phys. A. **501**, 729 (1989)
[57] H. Heiselberg, C. J. Pethick and D. G. Ravenhall, Ann. Phys. **223**, 37 (1993)
[58] S. L. Shapiro and S. A. Teukolsky, 'Black Holes, White Dwarfs, and Neutron Stars', John Wiley & Sons, New York, 1983
[59] S. Yamada, ApJ. **475**, 720 (1997)
[60] S. Yamada, H. -Th. Janka and H. Suzuki, Astron. & Astrophys. in press
[61] H. -Th. Janka, W. Keil and S. Yamada, in preparation
[62] K. Saito, T. Maruyama and K. Soutome, PRC. **40**, 407 (1989)

FIG. 1. The vector and axial vector structure functions $R_1(k_0, |\overrightarrow{\boldsymbol{k}}|)$ and $R_2(k_0, |\overrightarrow{\boldsymbol{k}}|)$ for the neutral current as functions of the transfer energy k_0. The density ρ_b, temperature T, proton fraction Y_p and the absolute value of the transferred three momentum $|\overrightarrow{\boldsymbol{k}}|$ are shown in the figure. The long dashed curve represents the non-interacting case, while the short dashed curve shows the case for the effective mass of the nucleon being taken into account. The solid curve shows the results of RPA.

FIG. 2. The vector and axial vector structure functions $R_1(k_0, |\overrightarrow{\boldsymbol{k}}|)$ and $R_2(k_0, |\overrightarrow{\boldsymbol{k}}|)$ for the neutral current as functions of the transfer energy k_0. The density ρ_b and proton fraction Y_p are the same as in Fig. 1, but the temperature T is smaller in this case, and the transferred three momentum $|\overrightarrow{\boldsymbol{k}}|$ is scaled as $\sim 3\,T$. The explicit values are shown in the figure.

FIG. 3. The vector and axial vector structure functions $R_1(k_0, |\overrightarrow{\boldsymbol{k}}|)$ and $R_2(k_0, |\overrightarrow{\boldsymbol{k}}|)$ for the neutral current as functions of the transfer energy k_0. The parameters are the same as in Fig. 1 but for the higher density, $\rho_b = 5 \times 10^{14}\mathrm{g/cm}^3$ as indicated in the figure.

FIG. 4. The vector and axial vector structure functions $R_1(k_0, |\overrightarrow{\boldsymbol{k}}|)$ and $R_2(k_0, |\overrightarrow{\boldsymbol{k}}|)$ for the neutral current as functions of the transfer energy k_0. The parameters are the same as Fig. 1 but for the different proton fraction $Y_p = 0.1$.

FIG. 5. The suppression factors for the total scattering rates, $R^{tot}(E_\nu^{in})$ defined in Eq. (3.3), from the expressions of Bruenn for vector currents (upper figure) and for axial vector currents (lower figure). Here E_ν^{in} is taken as $E_\nu^{in} = 3T$. The proton fraction is chosen as $Y_p = 0.3$. The suppressions are caused by the effective mass for nucleons and the effect of the transfer energy spectra instead of the δ-function.

FIG. 6. The suppression factors for the total scattering rates, $R^{tot}(E_\nu^{in})$ defined in Eq. (3.3), from the expressions of Bruenn for vector currents (upper figure) and for axial vector currents (lower figure). $E_\nu^{in} = 3T$ and $Y_p = 0.3$ are used here also as in Fig. 5. In this case, the suppressions are caused by the RPA correlations in addition to the effects considered in Fig. 5.

FIG. 7. The suppression factors for the total scattering rates, $R^{tot}(E_\nu^{in})$ defined in Eq. (3.3), from the expressions of Bruenn for vector currents (upper figure) and for axial vector currents (lower figure). The conditions are the same as those in Fig. 6, but the proton fraction is reduced here to $Y_p = 0.1$.

FIG. 8. The suppression factors for the total scattering rates, $R^{tot}(E_\nu^{in})$ defined in Eq. (3.3), from the expressions of Bruenn for vector currents (upper figure) and for axial vector currents (lower figure). The conditions are the same as those in Fig. 6, but the proton fraction is changed here to $Y_p = 0.5$.

FIG. 9. The structure functions $R_1(k_0, |\vec{\boldsymbol{k}}|)$ and $R_2(k_0, |\vec{\boldsymbol{k}}|)$ for the neutral current in the low density regime. The density ρ_b, temperature T, proton fraction Y_p and the absolute value of the transferred three momentum $|\vec{\boldsymbol{k}}|$ are shown in the figure. Only the effective mass of the nucleon is taken into account for the short dashed curve, while RPA is included for the solid curve.

FIG. 10. The enhancement factor for the vector current contribution (upper) and the suppression factor for the axial vector current part (lower) for $R^{tot}(E_\nu^{in})$ defined in Eq. (3.3) are shown for the low density regime. Here the proton fraction is $Y_p = 0.3$. The dark regions are outside the computational grid and roughly correspond to the coexistence phase of nucleons and nuclei, where a special care is required to treat the non-uniform matter.

FIG. 11. The structure functions $R_1(k_0, |\vec{\boldsymbol{k}}|)$ and $R_2(k_0, |\vec{\boldsymbol{k}}|)$ for the charged current reactions, where protons change into neutrons. The density ρ_b, temperature T, proton fraction Y_p and the absolute value of the transferred three momentum $|\vec{\boldsymbol{k}}|$ are shown in the figure. The long dashed curve represents the non-interacting case while the short dashed curve shows the case for the effective mass of the nucleon being taken into account. The solid curve shows the results of RPA.

FIG. 12. The structure functions $R_1(k_0, |\vec{\boldsymbol{k}}|)$ and $R_2(k_0, |\vec{\boldsymbol{k}}|)$ for the charged current reactions, where protons change into neutrons, for the proton fraction, $Y_p = 0.3$. The three momentum transfer $|\vec{\boldsymbol{k}}|$ is also changed to the electron chemical potential. The notations for curves are the same as in Fig. 11.

FIG. 13. The total ν_e emission rate defined in Eq. (3.9) as a function of the emitted neutrino energy E_ν^{out}. The upper panel shows the rate coming from the vector current and the lower panel represents the axial vector current contribution. The long dashed curves are obtained from the Bruenn's approximation formula, while the short dashed curves represent the results with the nucleon effective mass and the isovector potential being included. The solid curves correpond to the RPA results.

FIG. 14. The structure functions $R_1(k_0, |\vec{\boldsymbol{k}}|)$ and $R_2(k_0, |\vec{\boldsymbol{k}}|)$ for the charged current reactions, where protons change into neutrons. The density ρ_b, temperature T, proton fraction Y_p and the absolute value of the transferred three momentum $|\vec{\boldsymbol{k}}|$ are shown in the figure. The long dashed curve represents the non-interacting case while the short dashed curve shows the case for the effective mass of the nucleon being taken into account. The solid curve shows the results of RPA. Here the temperature is $T = 10$MeV. The three momentum transfer $|\vec{\boldsymbol{k}}|$ is also changed to the electron chemical potential. The notations for curves are the same as in Fig. 11.

FIG. 15. The total ν_e emission rate defined in Eq. (3.9) as a function of the emitted neutrino energy E_ν^{out}. The upper panel shows the rate coming from the vector current and the lower panel represents the axial vector current contribution. The long dashed curves are obtained from the Bruenn's approximation formula, while the short dashed curves represent the results with the nucleon effective mass and the isovector potential being included. The solid curves correpond to the RPA results. Here the temperature is $T = 10$MeV.

FIG. 16. The total ν_e emission rate defined in Eq. (3.9) as a function of the emitted neutrino energy E_ν^{out}. The upper panel shows the rate coming from the vector current and the lower panel represents the axial vector current contribution. The long dashed curves are obtained from the Bruenn's approximation formula, while the short dashed curves represent the results with the nucleon effective mass and the isovector potential being included. The solid curves correpond to the RPA results. Here the density is $\rho_b = 5 \times 10^{14}\mathrm{g/cm}^3$

FIG. 17. The total ν_e emission rate defined in Eq. (3.9) as a function of the emitted neutrino energy E_ν^{out}. The upper panel shows the rate coming from the vector current and the lower panel represents the axial vector current contribution. The long dashed curves are obtained from the Bruenn's approximation formula, while the short dashed curves represent the results with the nucleon effective mass and the isovector potential being included. The solid curves correpond to the RPA results. Here the proton fraction is $Y_p = 0.1$.

FIG. 18. The structure functions $R_1(k_0, |\overrightarrow{\boldsymbol{k}}|)$ and $R_2(k_0, |\overrightarrow{\boldsymbol{k}}|)$ for the charged current reactions, where neutrons change into protons. The density ρ_b, temperature T, proton fraction Y_p and the absolute value of the transferred three momentum $|\boldsymbol{k}|$ are shown in the figure. The long dashed curve represents the non-interacting case while the short dashed curve shows the case for the effective mass and the isovector potential of the nucleon being taken into account. The solid curve shows the results of RPA.

FIG. 19. The total $\overline{\nu}_e$ emission rate as a function of the emitted neutrino energy E_ν^{out}. The upper panel shows the rate coming from the vector current and the lower panel represents the axial vector current contribution. The long dashed curves are obtained from the Bruenn's approximation formula, the short dashed curves represent the results with the nucleon effective mass and the isovector potential being included. The solid curves display the RPA results.

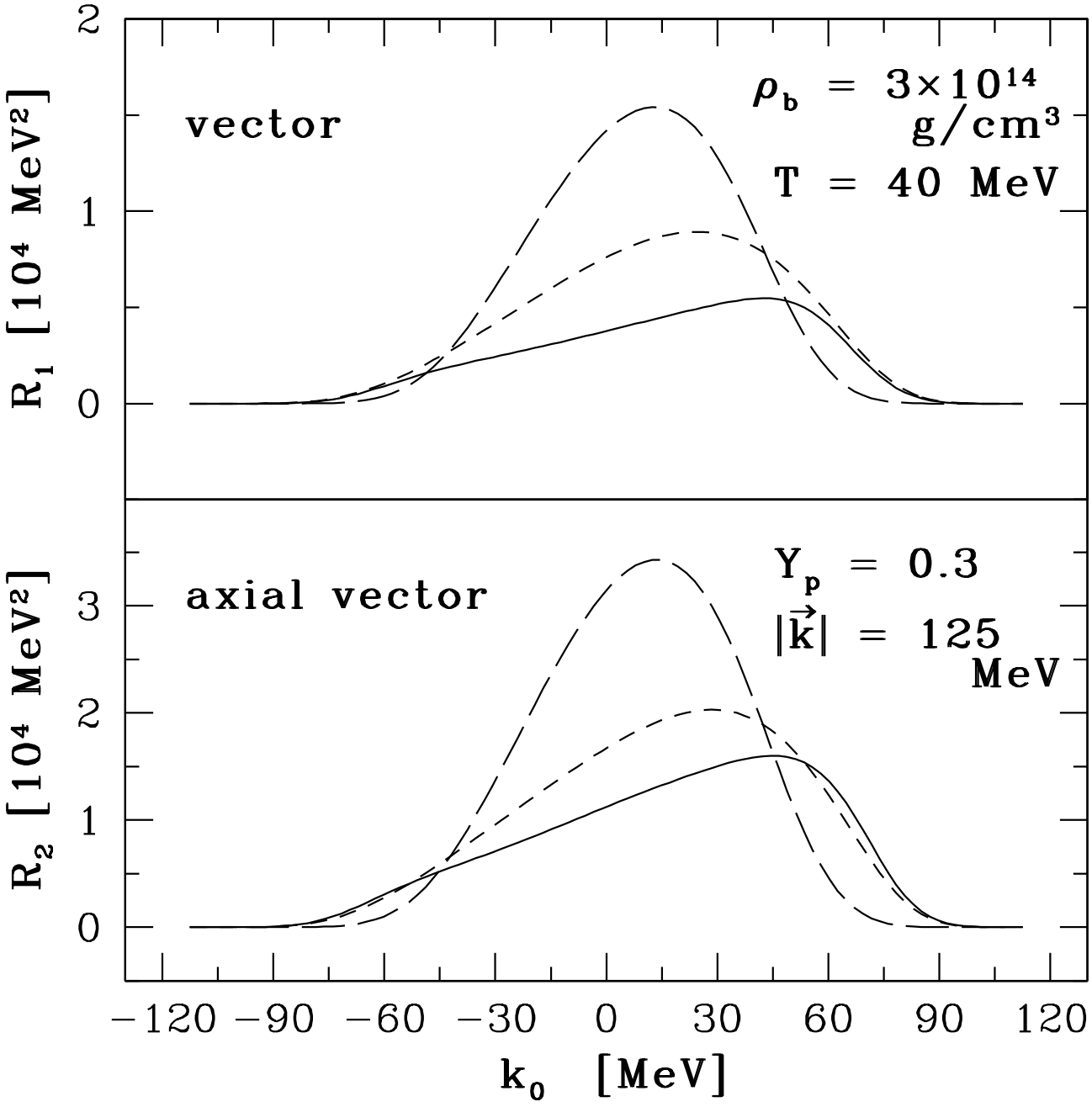
vector
ρ_b = 3×10¹⁴ g/cm³
T = 40 MeV
R_1 [10⁴ MeV²]
axial vector
Y_p = 0.3
$|\vec{k}|$ = 125 MeV
R_2 [10⁴ MeV²]
k_0 [MeV]

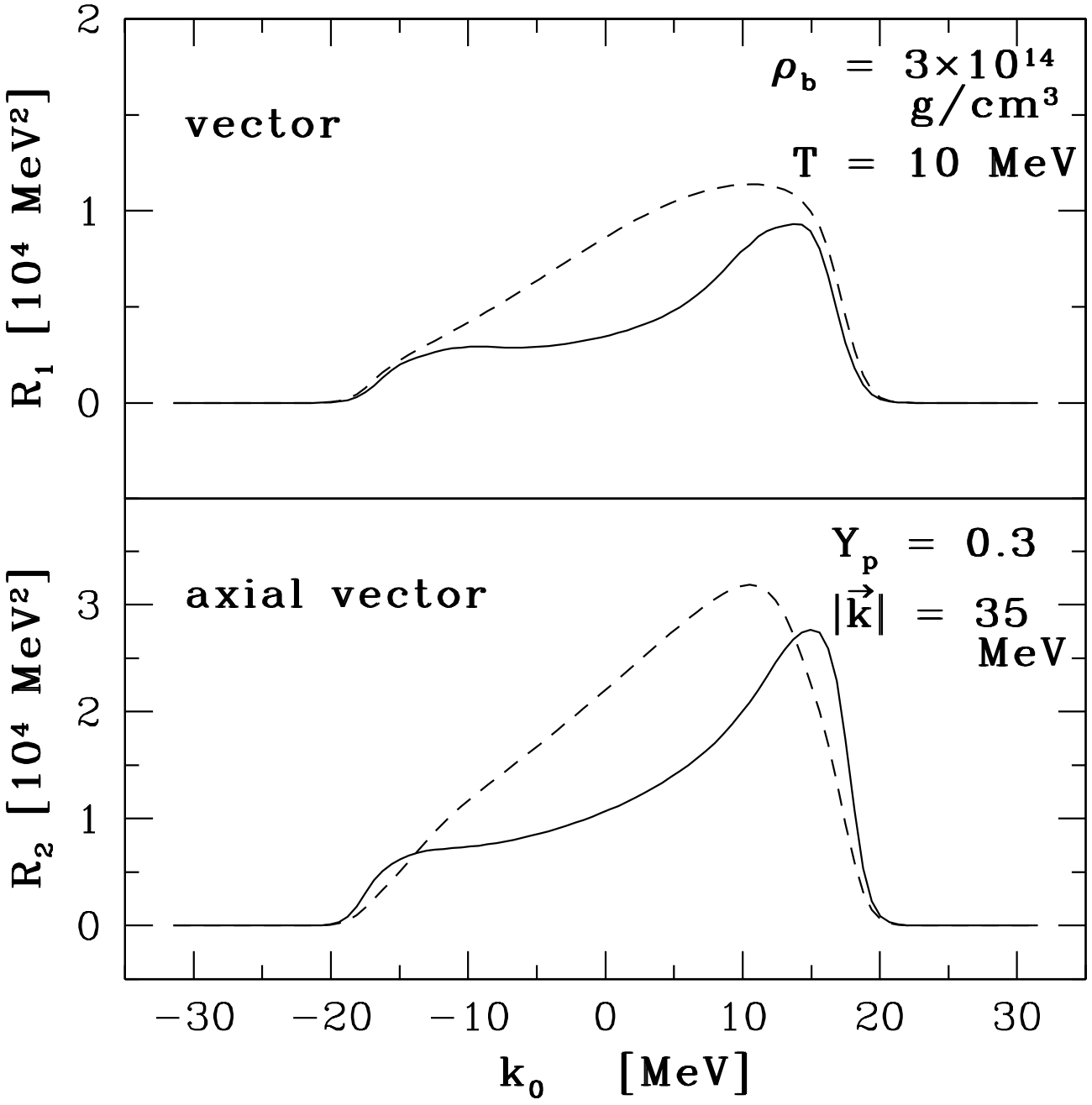
vector
$\rho_b = 3\times10^{14}$ g/cm^3
T = 10 MeV
R_1 [10^4 MeV^2]
axial vector
Y_p = 0.3
$|\vec{k}|$ = 35 MeV
R_2 [10^4 MeV^2]
k_0 [MeV]

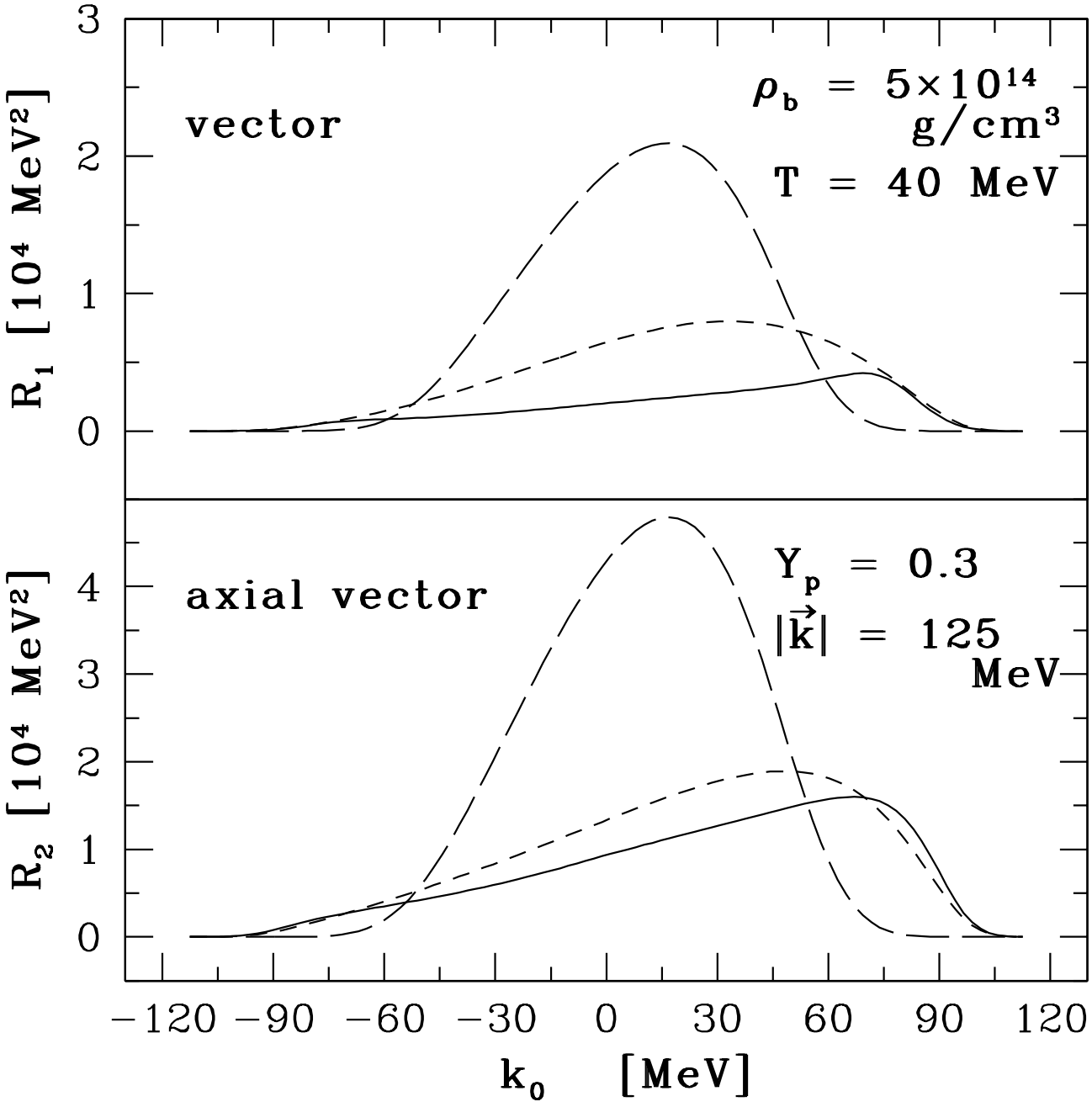
vector
ρ_b = 5×10¹⁴ g/cm³
T = 40 MeV
R_1 [10⁴ MeV²]
axial vector
Y_p = 0.3
$|\vec{k}|$ = 125 MeV
R_2 [10⁴ MeV²]
k_0 [MeV]

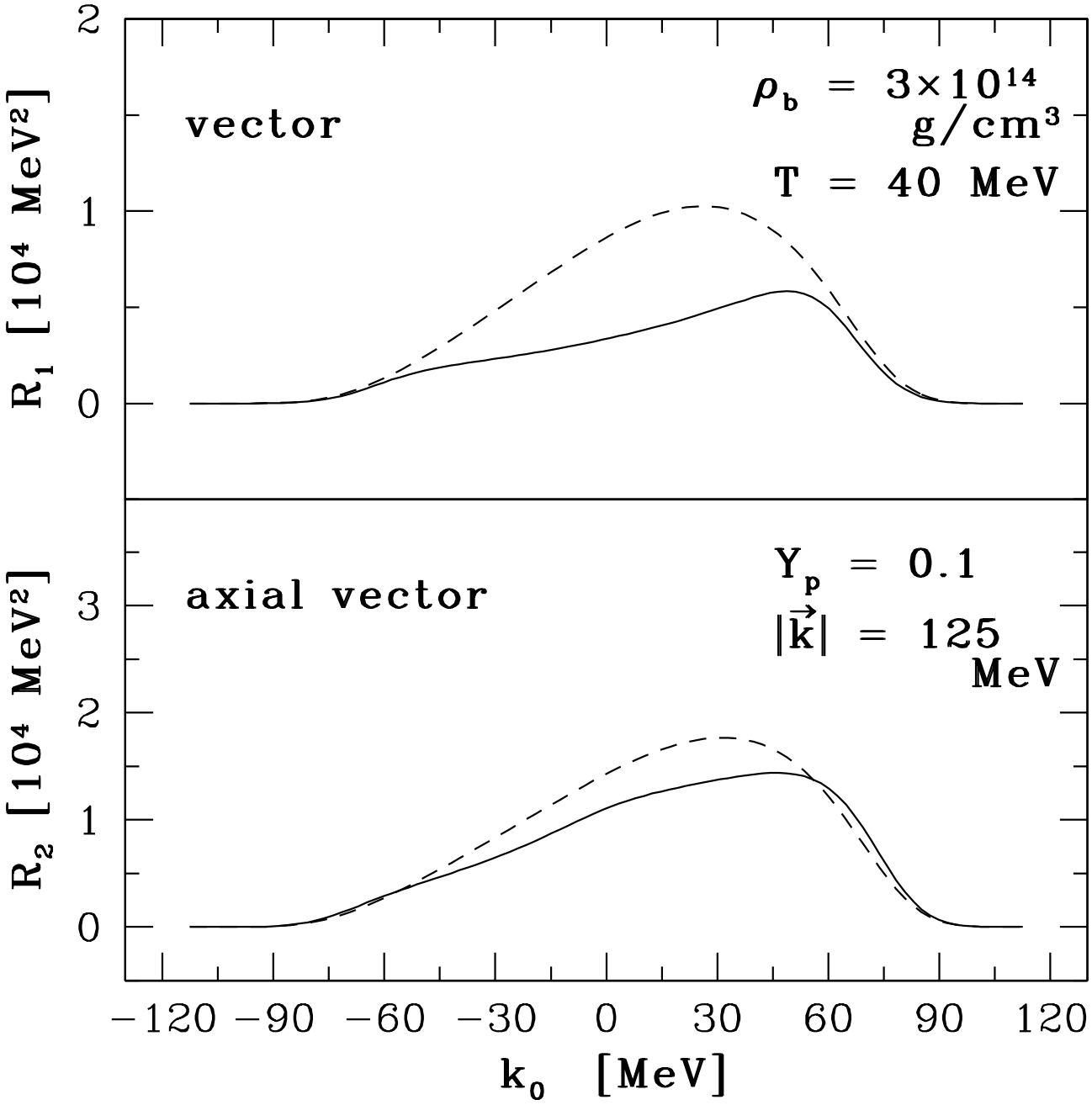
vector
$\rho_b = 3\times10^{14}$ g/cm^3
T = 40 MeV
R_1 [10^4 MeV^2]
2
1
0
axial vector
$Y_p = 0.1$
$|\vec{k}| = 125$ MeV
R_2 [10^4 MeV^2]
3
2
1
0
−120 −90 −60 −30 0 30 60 90 120
k_0 [MeV]

Suppression Factor for R_1^{tot} ($Y_p = 0.3$)

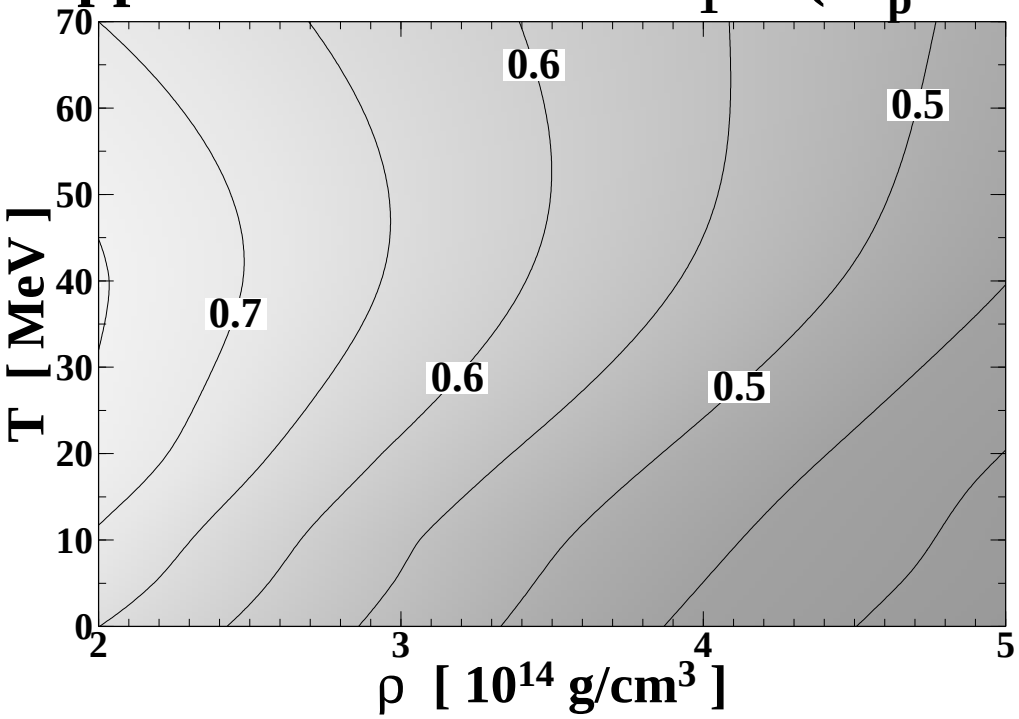

Suppression Factor for R_2^{tot} ($Y_p = 0.3$)

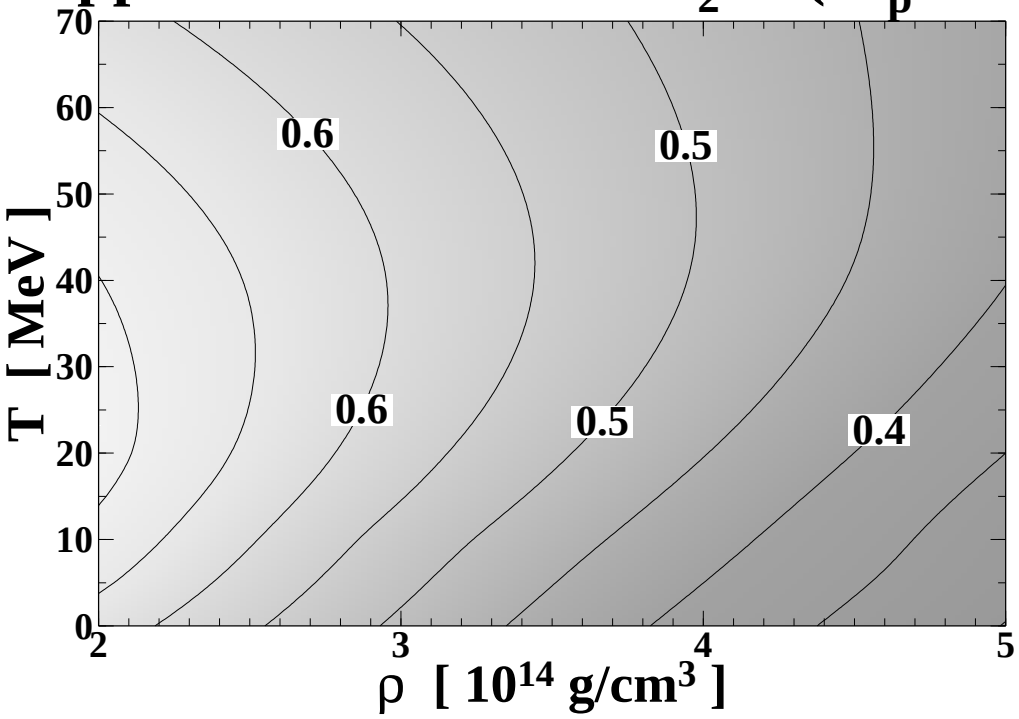

Suppression Factor for R_1^{tot} ($Y_p = 0.3$)

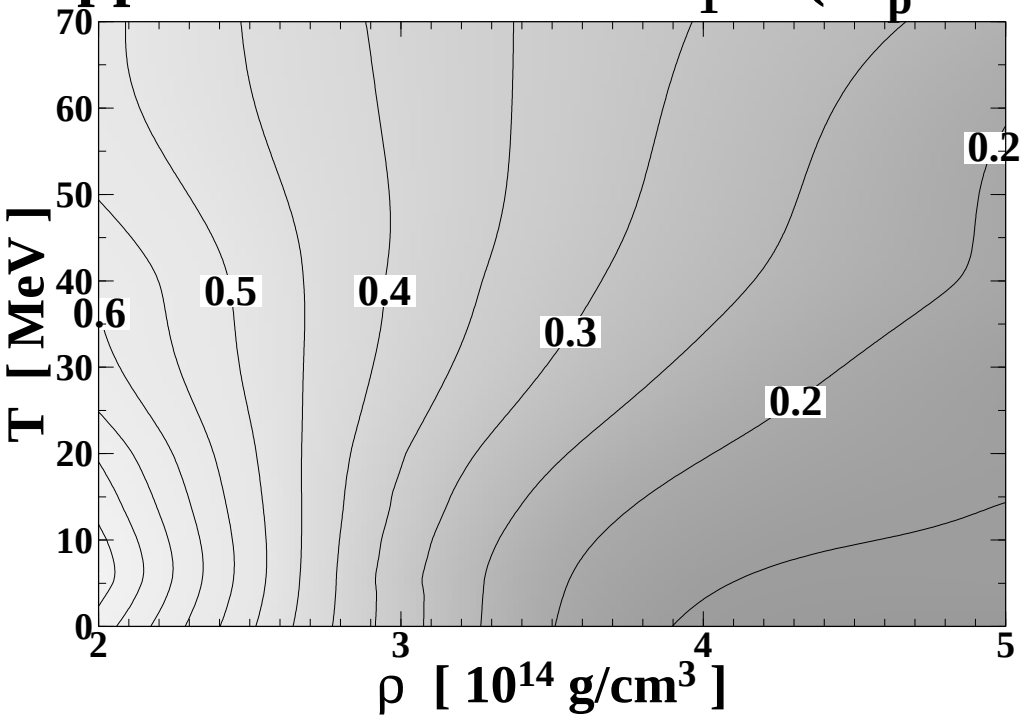

Suppression Factor for R_2^{tot} ($Y_p = 0.3$)

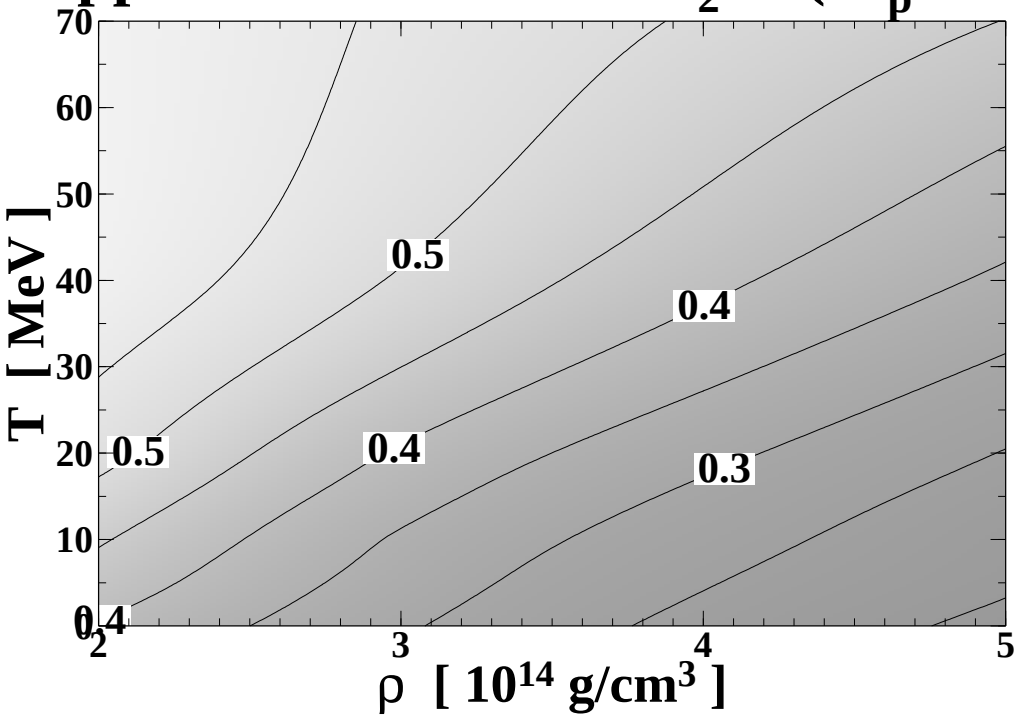

Suppression Factor for R_1^{tot} ($Y_p = 0.1$)

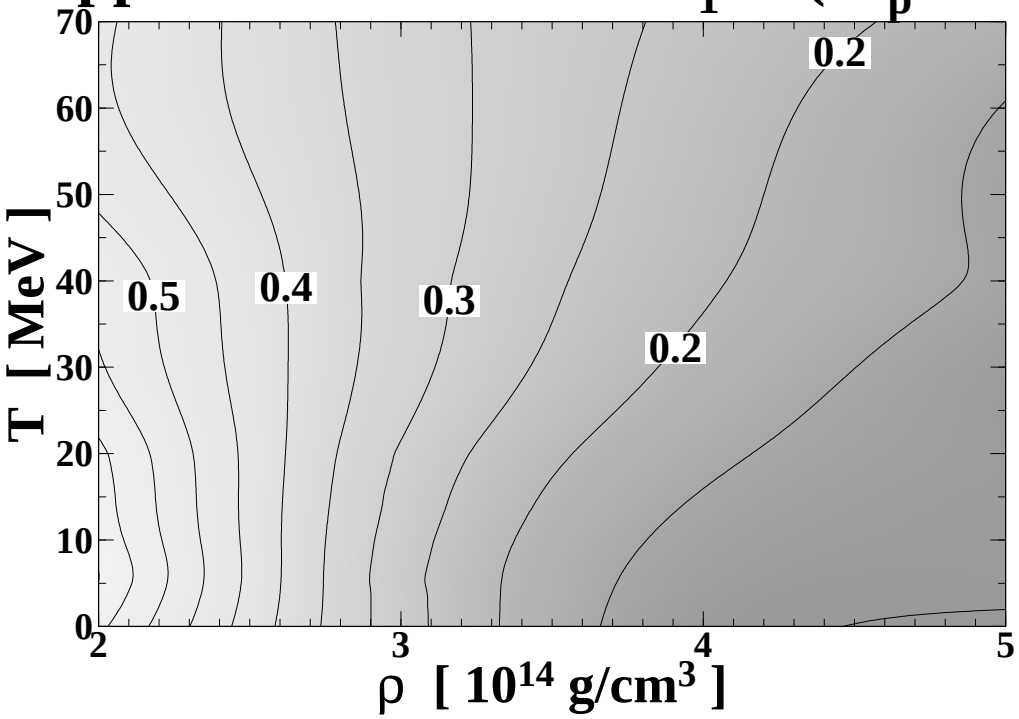

Suppression Factor for R_2^{tot} ($Y_p = 0.1$)

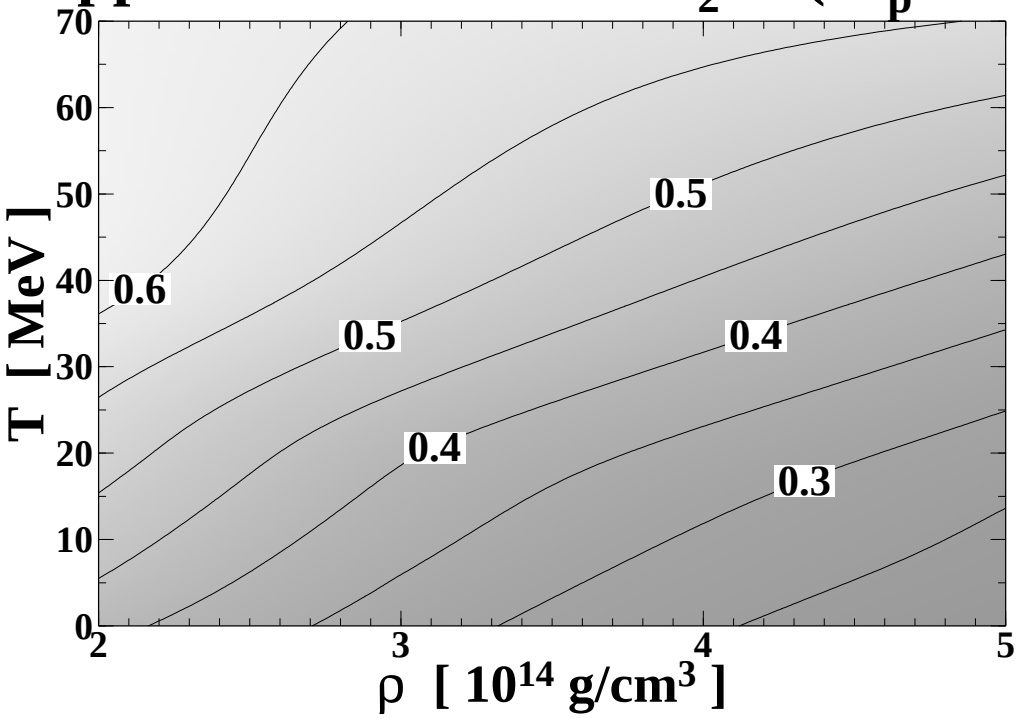

Suppression Factor for R_1^{tot} ($Y_p = 0.5$)

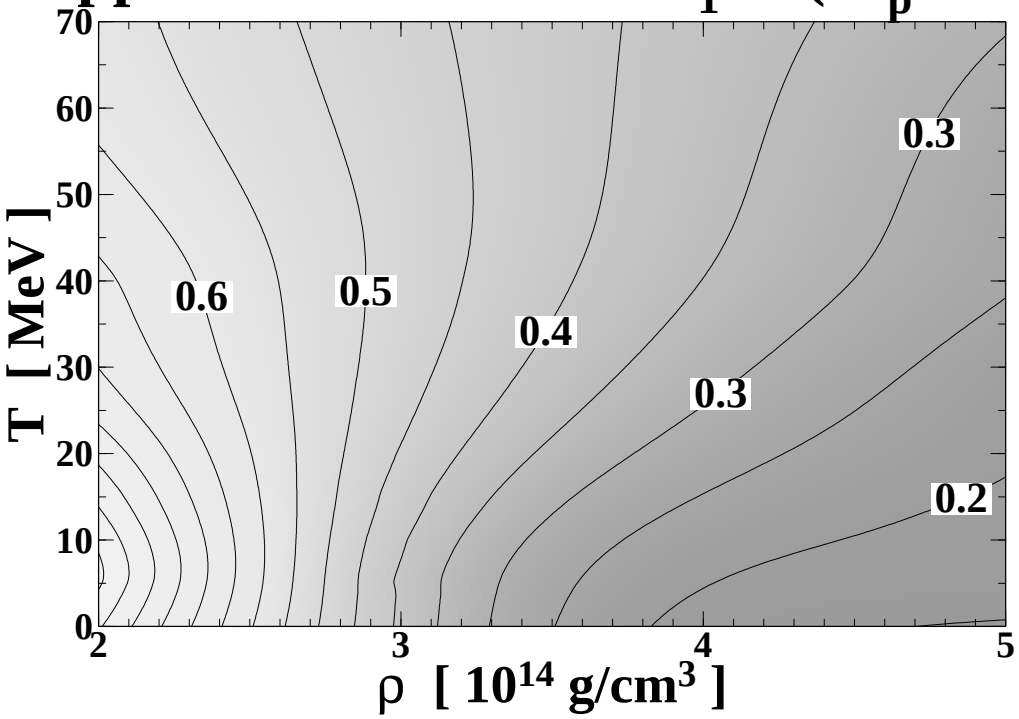

Suppression Factor for R_2^{tot} ($Y_p = 0.5$)

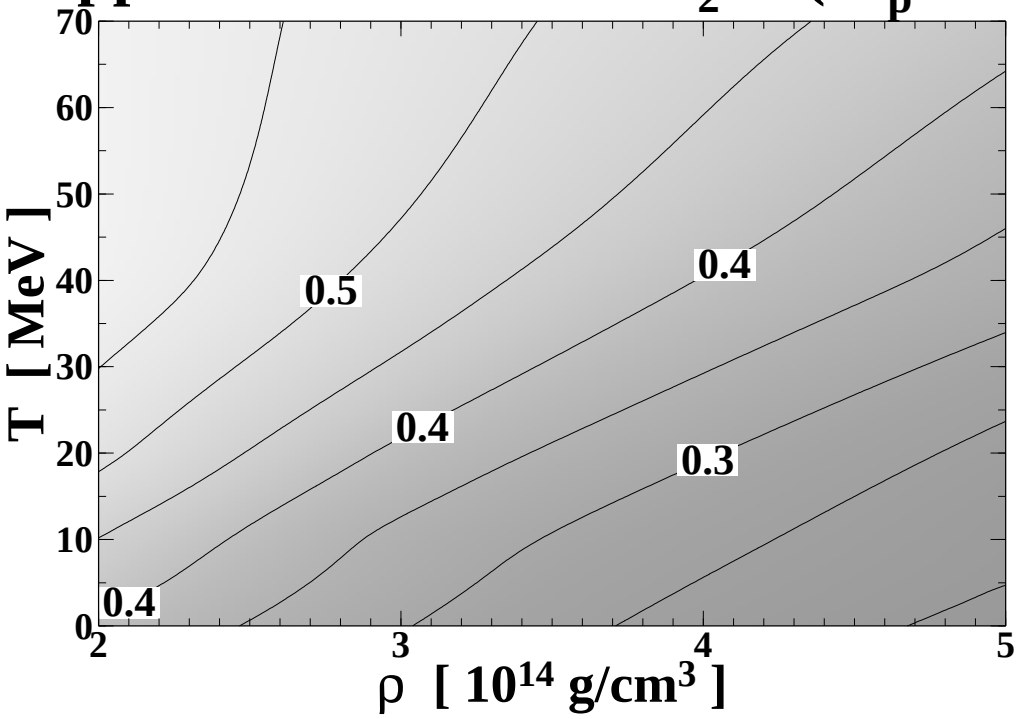

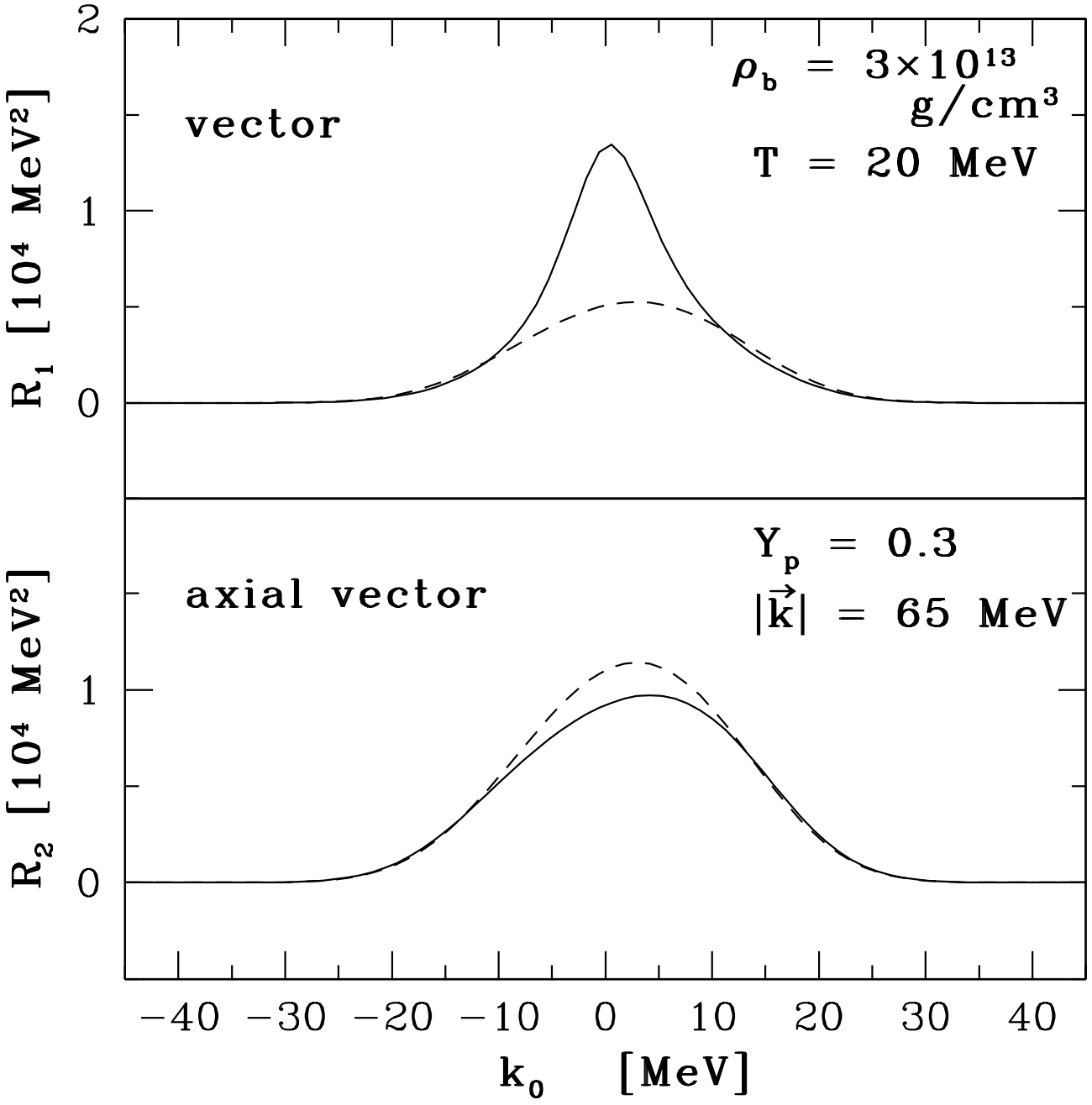
vector
$\rho_b = 3\times10^{13}$ g/cm^3
T = 20 MeV
R_1 [10^4 MeV^2]
2
1
0
axial vector
Y_p = 0.3
$|\vec{k}|$ = 65 MeV
R_2 [10^4 MeV^2]
1
0
−40 −30 −20 −10 0 10 20 30 40
k_0 [MeV]

Enhancement Factor for R_1^{tot} ($Y_p = 0.3$)

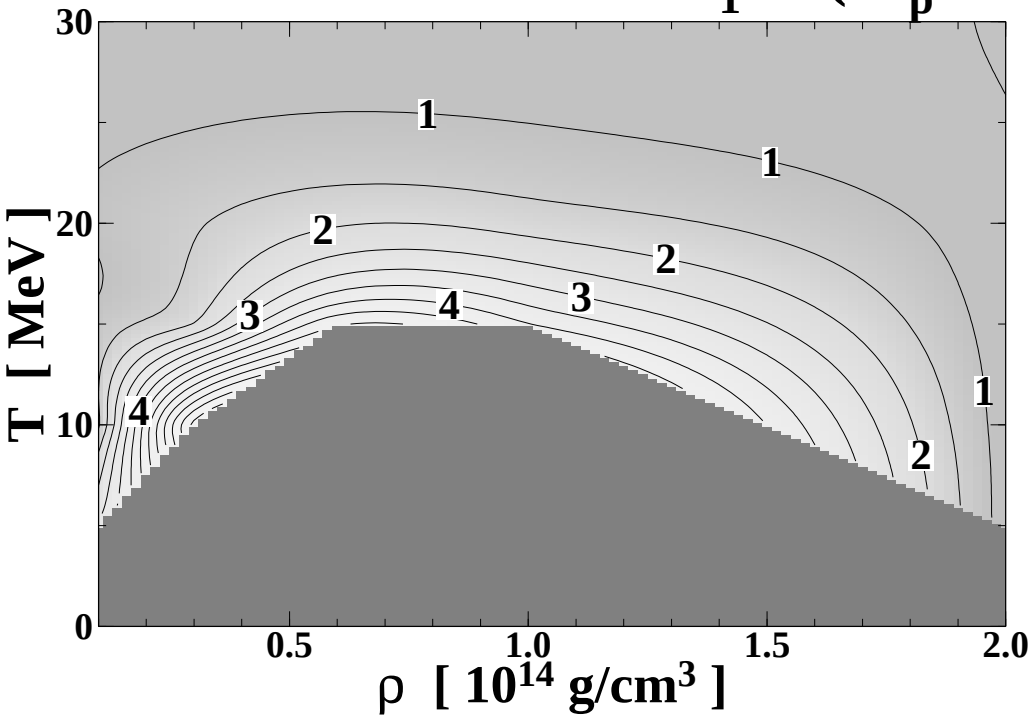

Suppression Factor for R_2^{tot} ($Y_p = 0.3$)

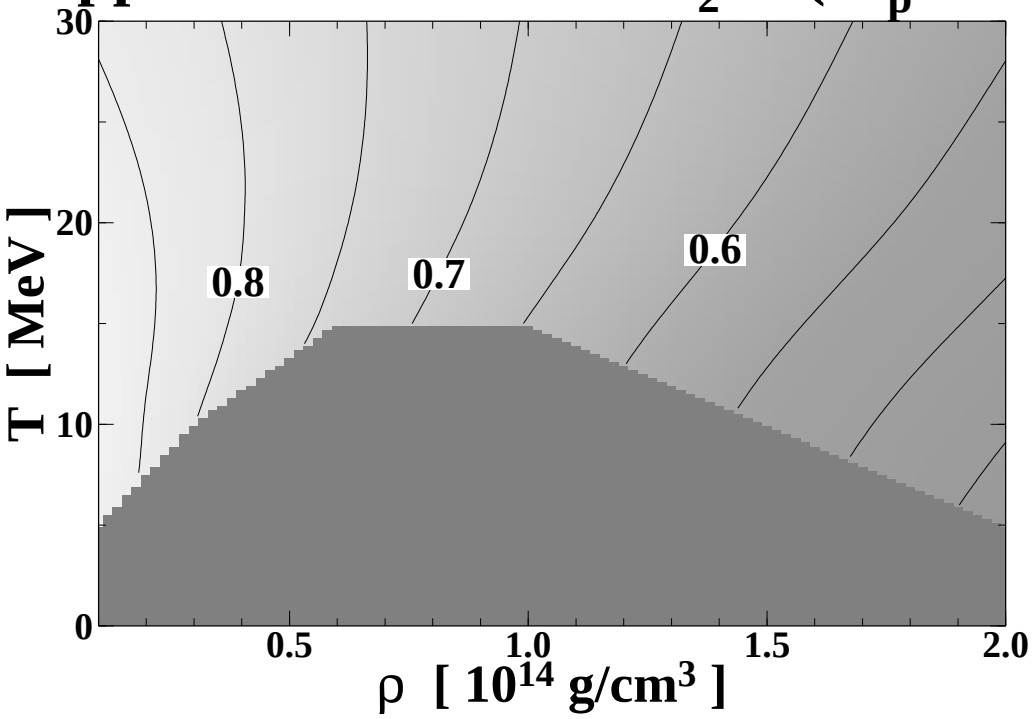

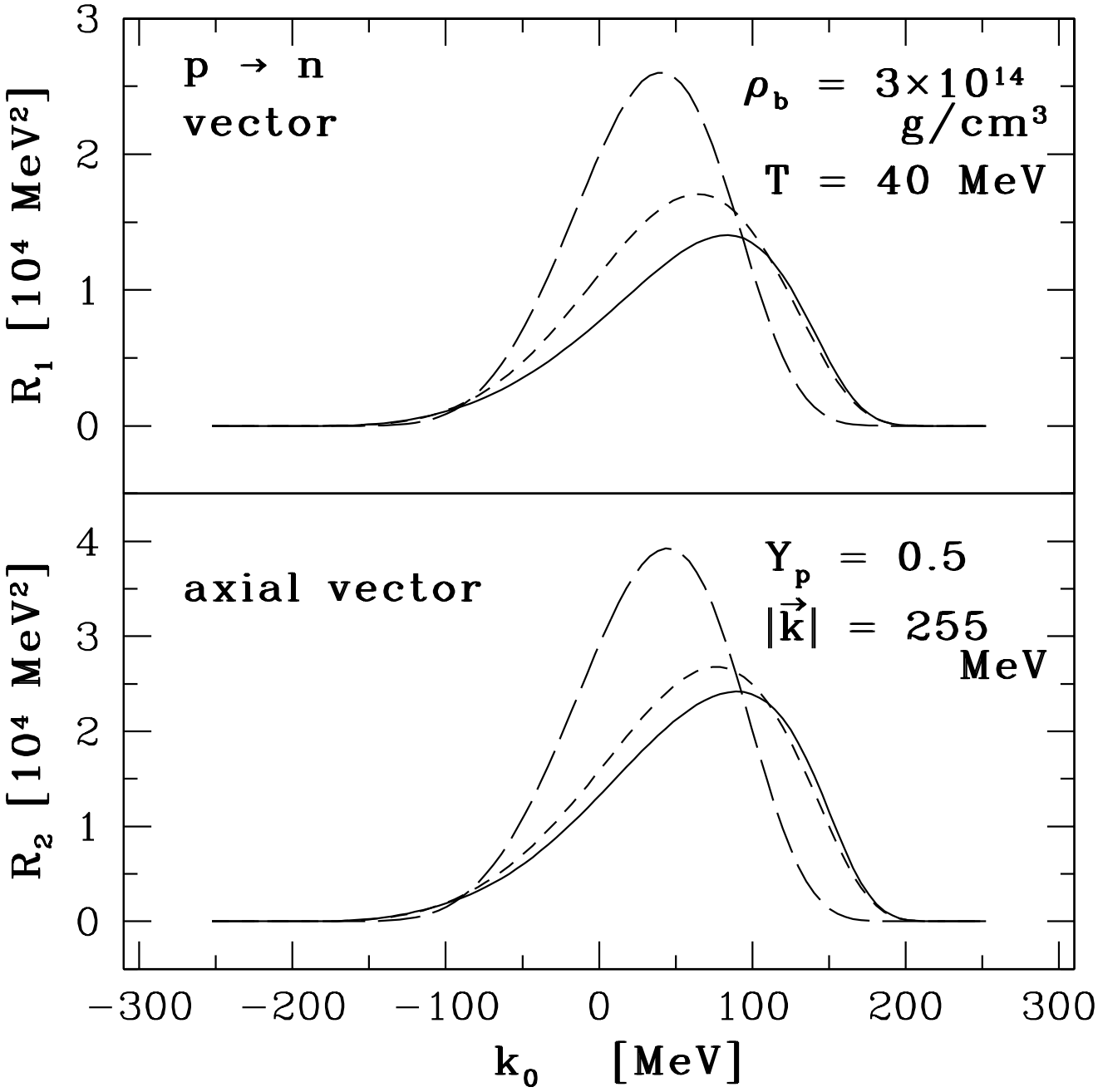
p → n
vector
ρ_b = 3×10¹⁴ g/cm³
T = 40 MeV
R_1 [10⁴ MeV²]
axial vector
Y_p = 0.5
$|\vec{k}|$ = 255 MeV
R_2 [10⁴ MeV²]
k_0 [MeV]

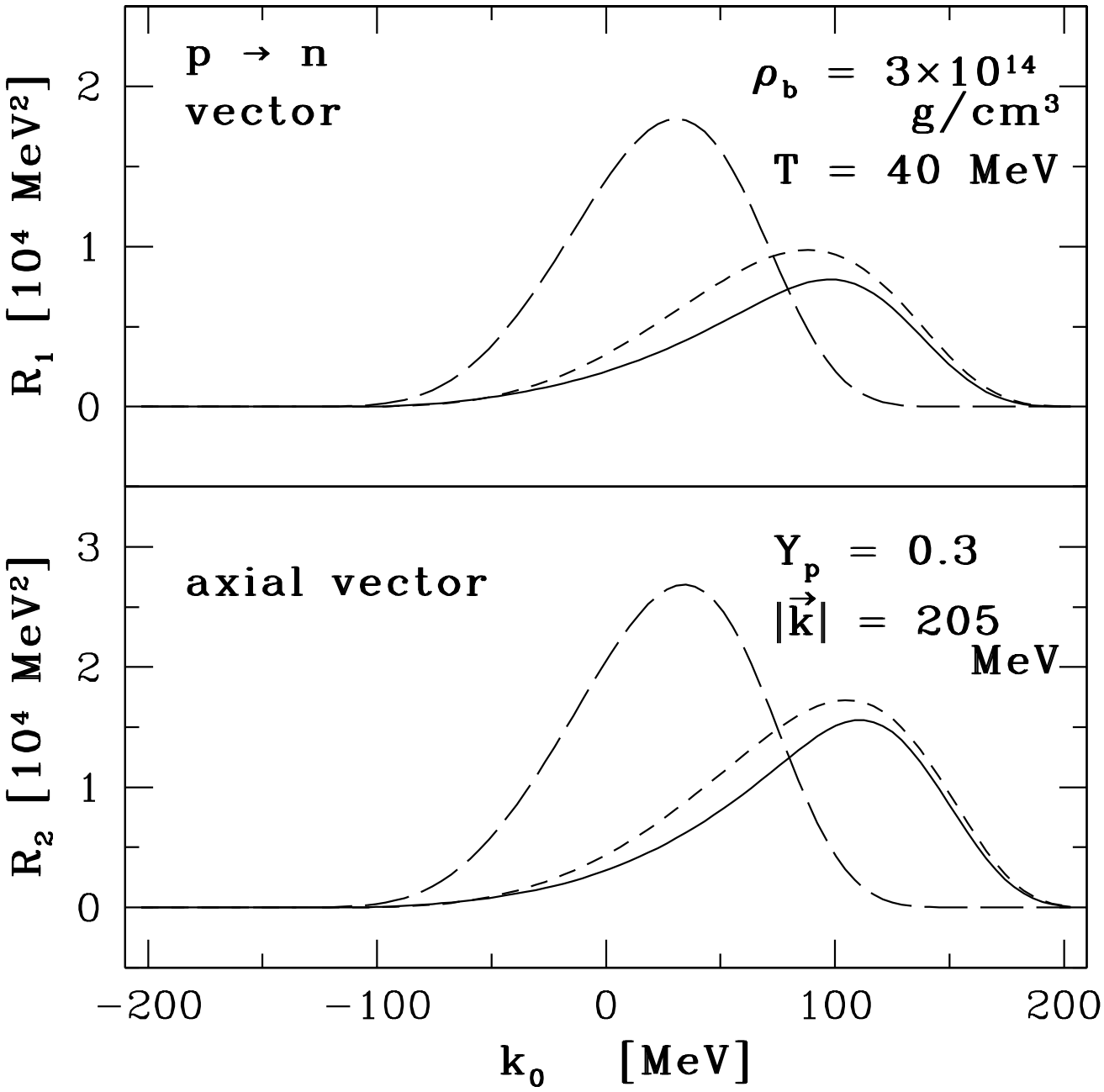
p → n
vector
ρ_b = 3×10¹⁴ g/cm³
T = 40 MeV
R_1 [10⁴ MeV²]
axial vector
Y_p = 0.3
$|\vec{k}|$ = 205 MeV
R_2 [10⁴ MeV²]
k_0 [MeV]

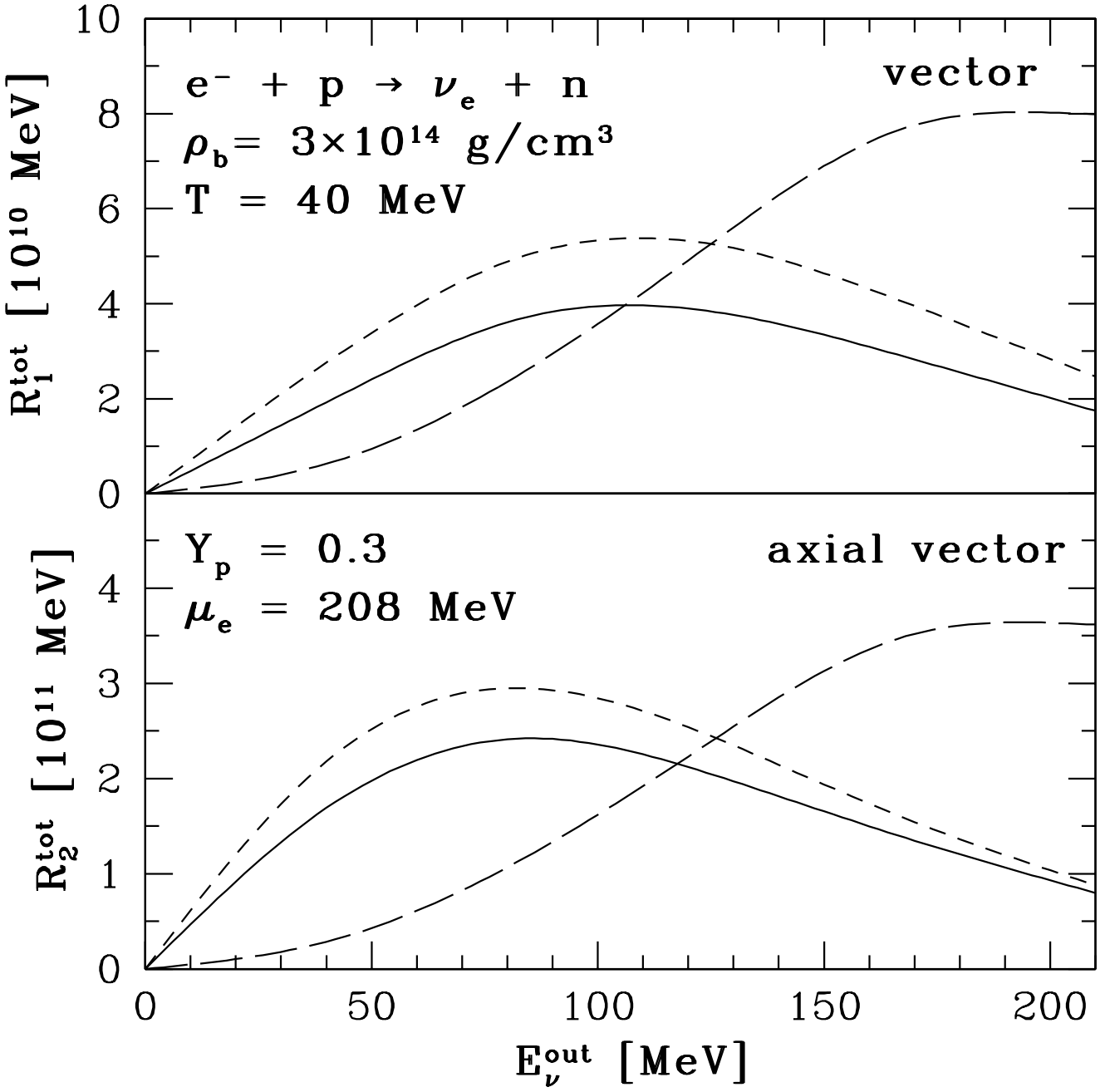
e⁻ + p → ν_e + n
ρ_b = 3×10¹⁴ g/cm³
T = 40 MeV
vector
Y_p = 0.3
μ_e = 208 MeV
axial vector
R₁^tot [10¹⁰ MeV]
R₂^tot [10¹¹ MeV]
E_ν^out [MeV]
0
2
4
6
8
10
1
3
50
100
150
200

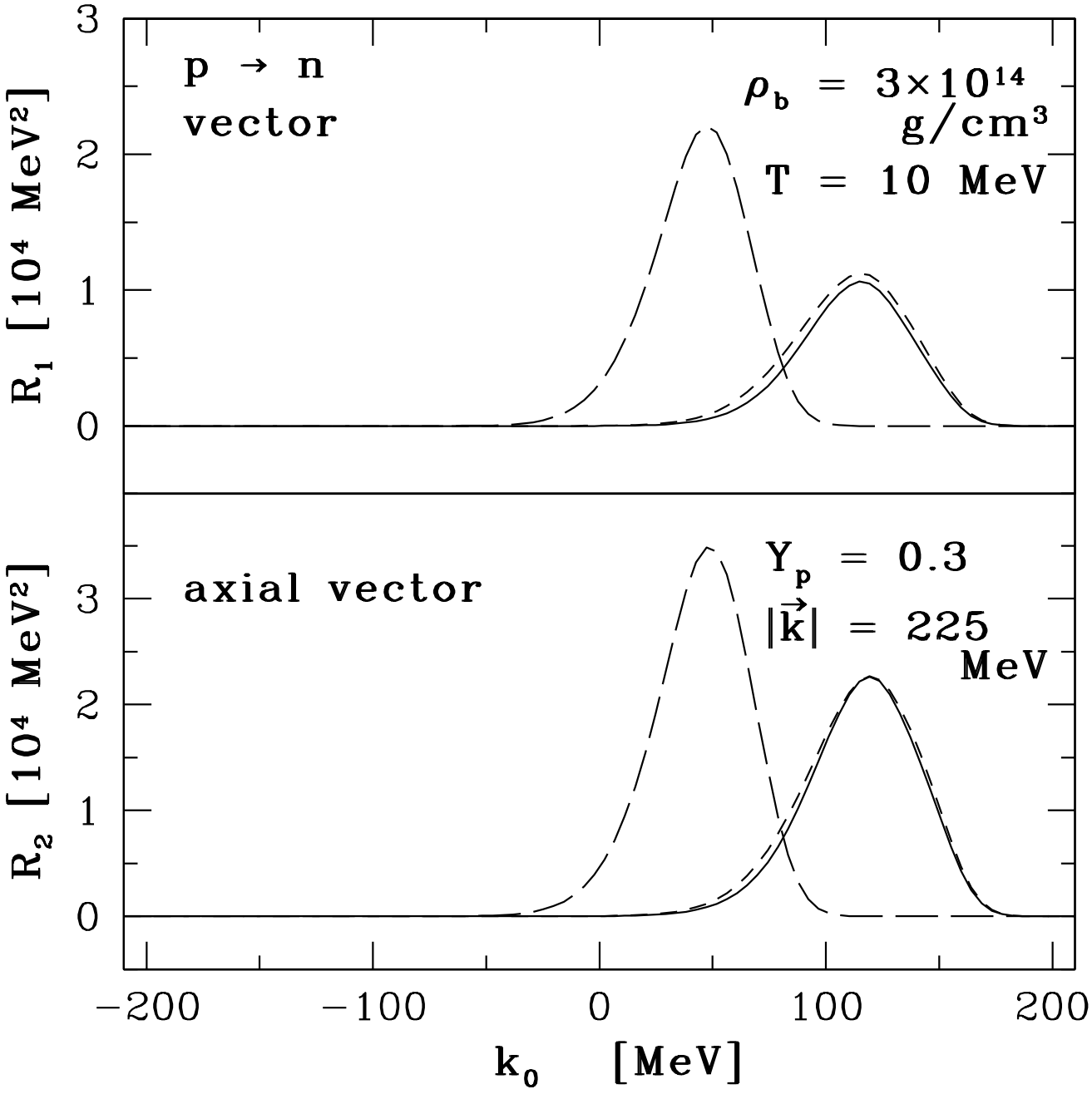
p → n
vector
ρ_b = 3×10¹⁴ g/cm³
T = 10 MeV
R_1 [10⁴ MeV²]
axial vector
Y_p = 0.3
$|\vec{k}|$ = 225 MeV
R_2 [10⁴ MeV²]
0
1
2
3
−200
−100
0
100
200
k_0 [MeV]

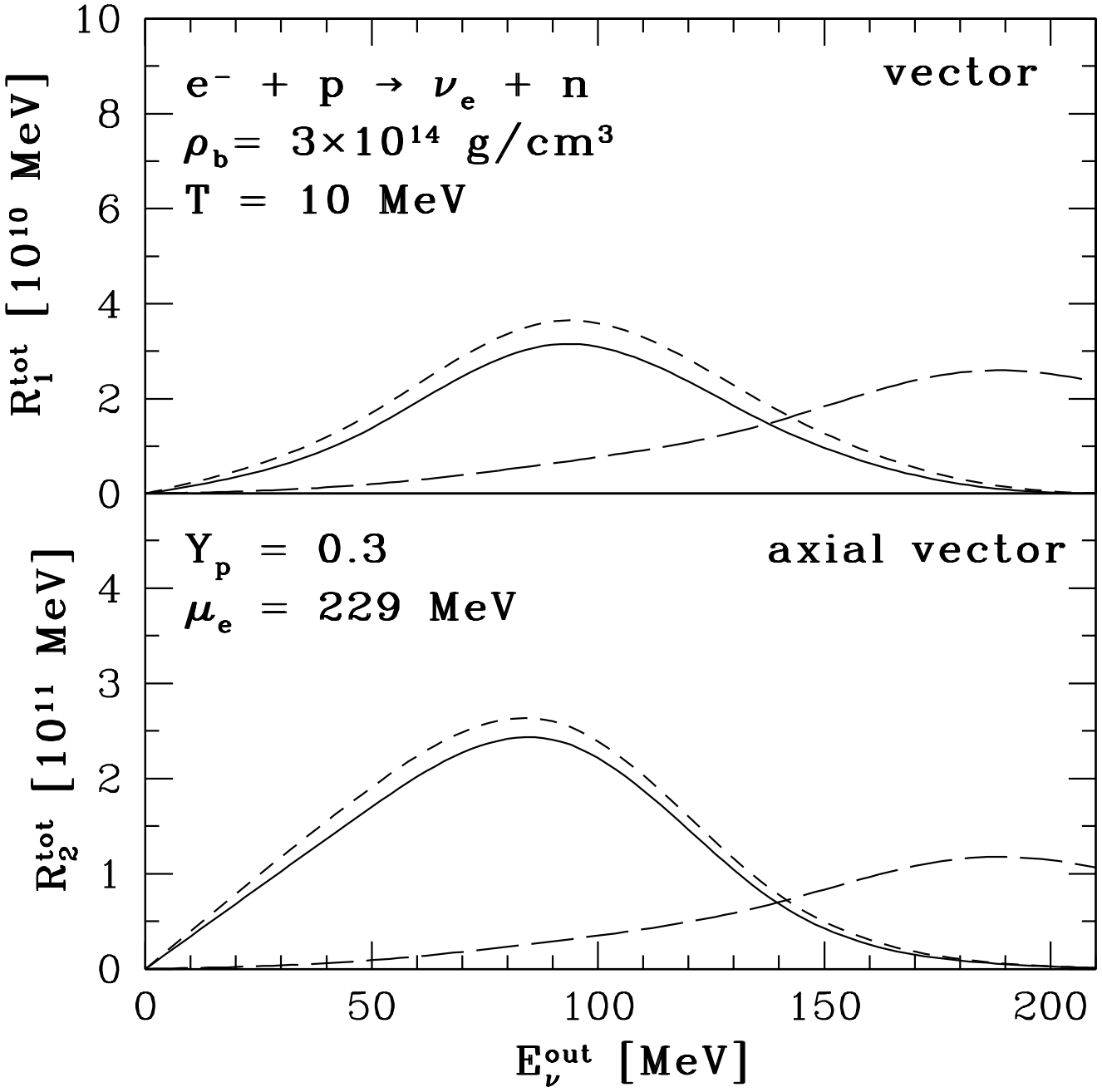
e⁻ + p → ν_e + n
ρ_b = 3×10¹⁴ g/cm³
T = 10 MeV
vector
R₁^tot [10¹⁰ MeV]
Y_p = 0.3
μ_e = 229 MeV
axial vector
R₂^tot [10¹¹ MeV]
E_ν^out [MeV]
0
50
100
150
200
2
4
6
8
10
1
3

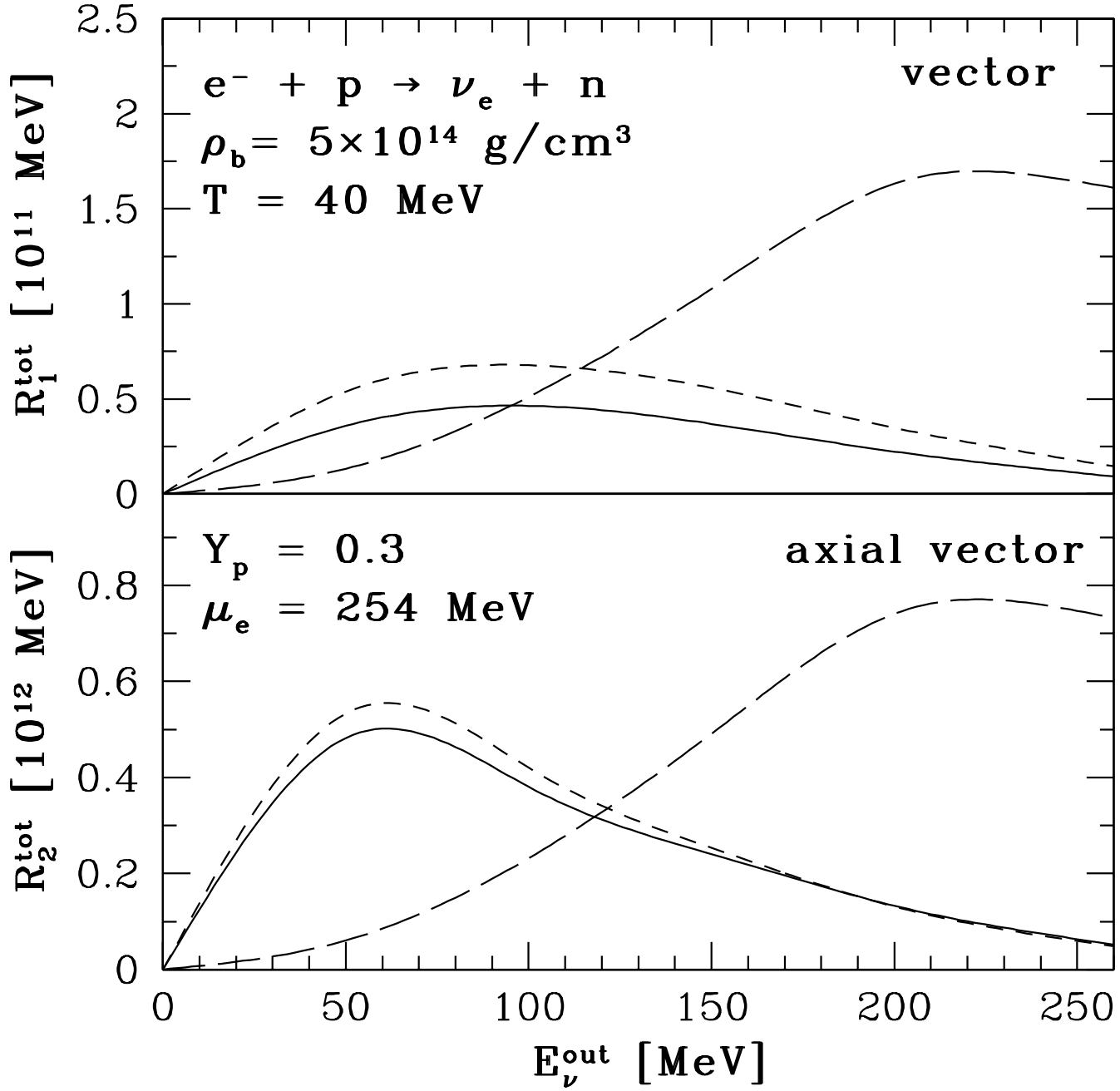
e⁻ + p → ν_e + n
ρ_b = 5×10¹⁴ g/cm³
T = 40 MeV
vector
Y_p = 0.3
μ_e = 254 MeV
axial vector
R₁^tot [10¹¹ MeV]
R₂^tot [10¹² MeV]
E_ν^out [MeV]
0
0.5
1
1.5
2
2.5
0.2
0.4
0.6
0.8
50
100
150
200
250

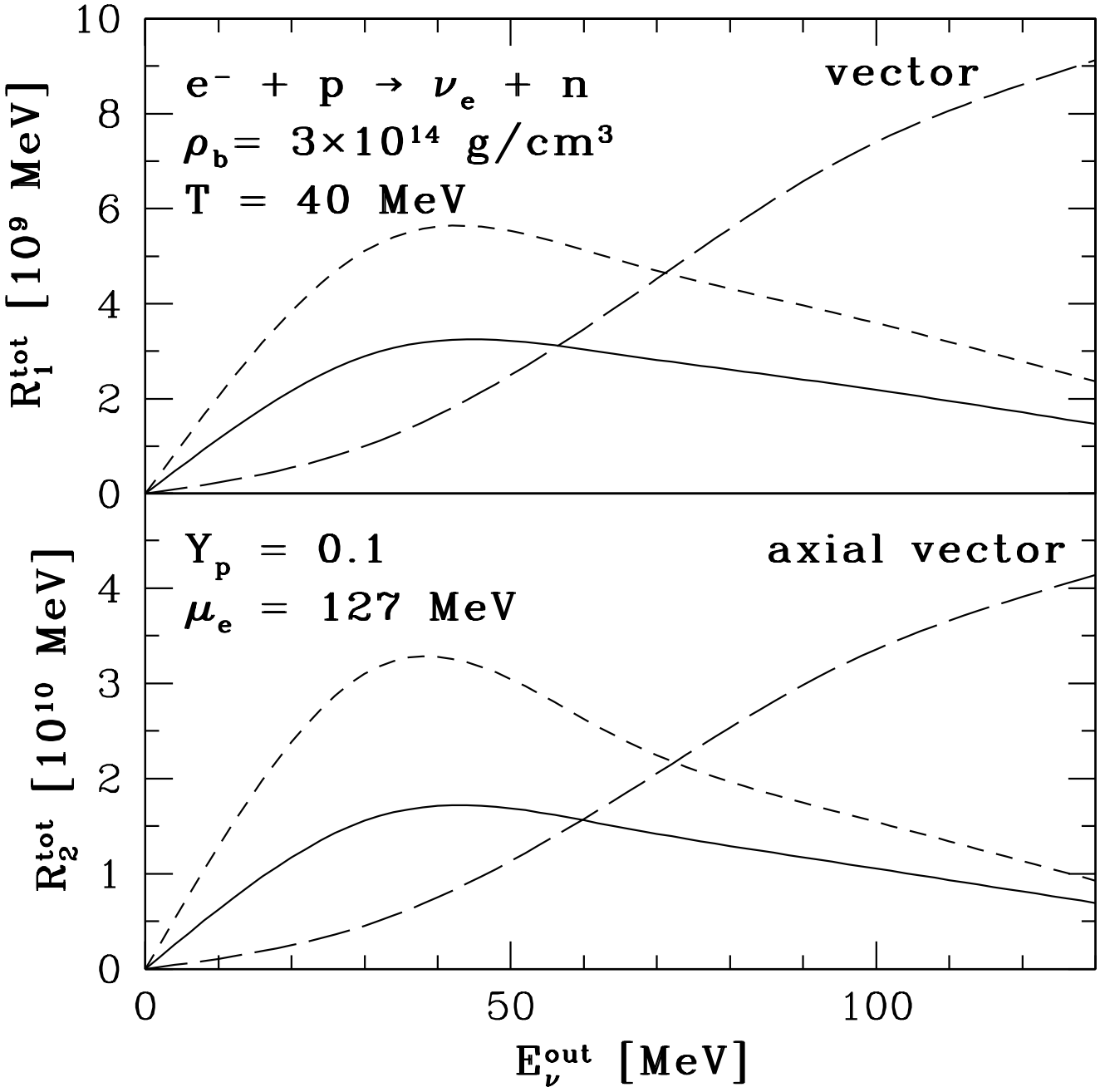
e⁻ + p → ν_e + n
ρ_b = 3×10¹⁴ g/cm³
T = 40 MeV
vector
Y_p = 0.1
μ_e = 127 MeV
axial vector
R₁^tot [10⁹ MeV]
R₂^tot [10¹⁰ MeV]
E_ν^out [MeV]
0
2
4
6
8
10
1
3
50
100

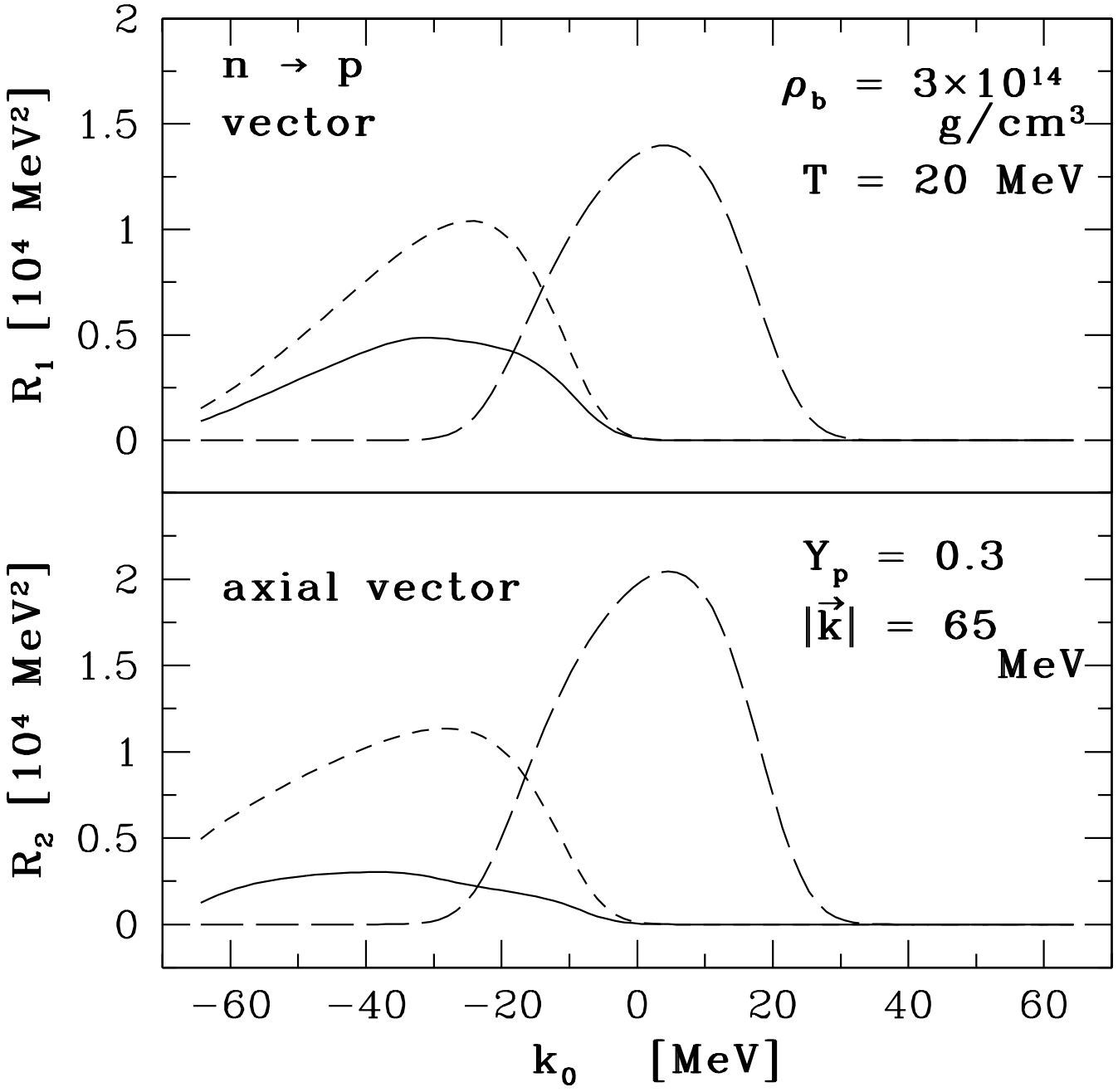
n → p
vector
ρ_b = 3×10¹⁴ g/cm³
T = 20 MeV
R_1 [10⁴ MeV²]
axial vector
Y_p = 0.3
$|\vec{k}|$ = 65 MeV
R_2 [10⁴ MeV²]
0
0.5
1
1.5
2
−60
−40
−20
0
20
40
60
k_0 [MeV]

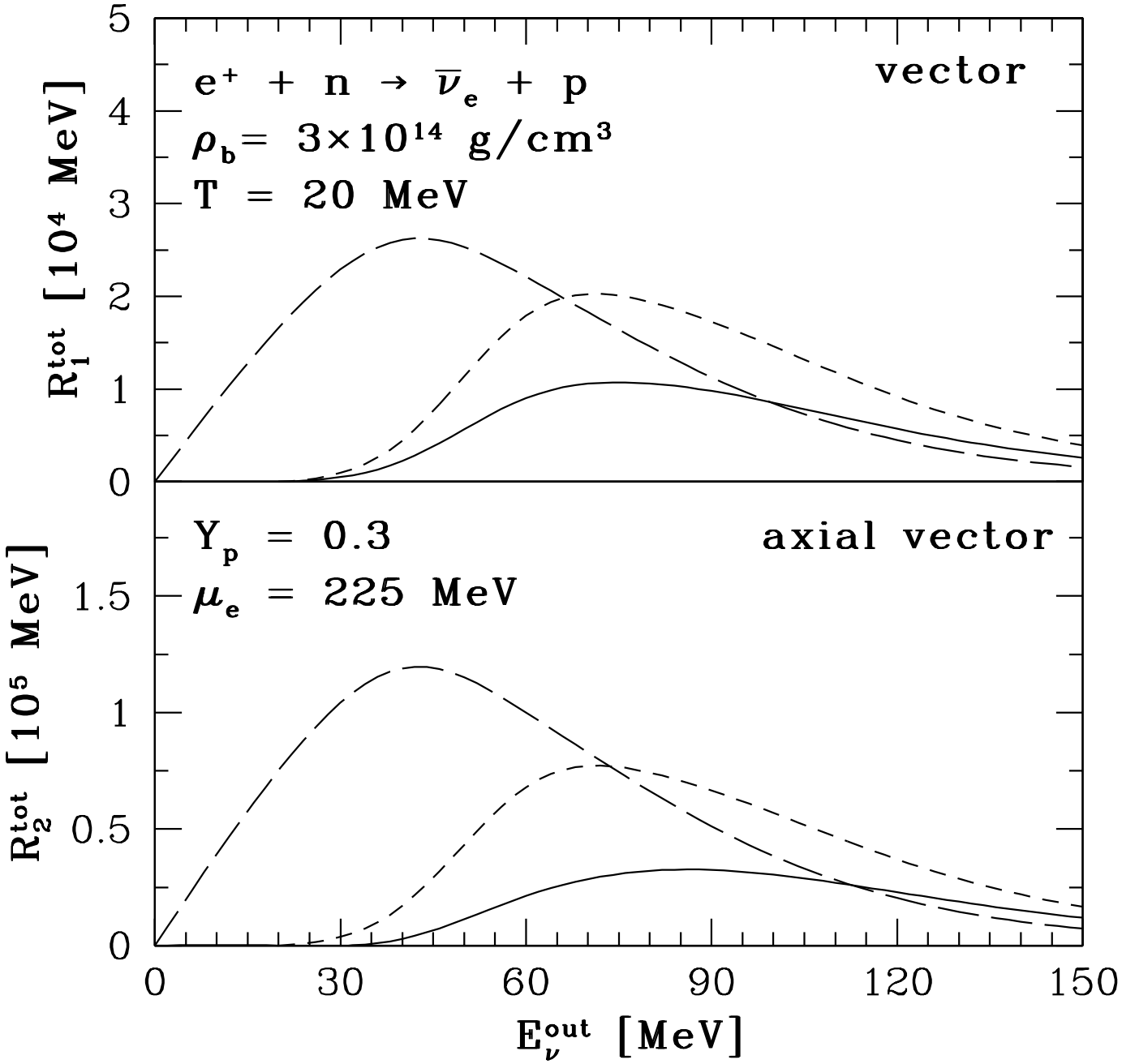
$e^+ + n \rightarrow \bar{\nu}_e + p$
vector
$\rho_b = 3\times10^{14}$ g/cm^3
T = 20 MeV
R_1^{tot} [10^4 MeV]
Y_p = 0.3
axial vector
μ_e = 225 MeV
R_2^{tot} [10^5 MeV]
0
30
60
90
120
150
E_ν^{out} [MeV]